ORIGINAL ARTICLE

Immune-awakening *Saccharomyces*-inspired nanocarrier for oral target delivery to lymph and tumors

Yuling Mao[a], Xiudan Wang[a], Caishun Chen[a], Qinfu Zhao[a], Yanfeng Liu[c], Jinghai Zhang[b],*, Siling Wang[a],*

[a]Department of Pharmaceutics, School of Pharmacy, Shenyang Pharmaceutical University, Shenyang 110016, China
[b]Department of Biomedical Engineering, School of Medical Devices, Shenyang Pharmaceutical University, Shenyang 110016, China
[c]School of Life Science and Bio-pharmaceutics, Shenyang Pharmaceutical University, Shenyang 110016, China

Abstract   Utilization of the intestinal lymphatic pathway will allow extraordinary gains in lymph and tumors cascade-targeted delivery of oral drugs and awakening the innate/adaptive immunity of the body and the lesion microenvironment, in addition to improving oral bioavailability relative to other means of delivery of oral drugs. Here, inspired by the specific invasion route of intestinal microorganisms, we pioneered an immune-awakening *Saccharomyces*-inspired mesoporous silicon nanoparticle (yMSN) for the ingenious cascade-targeted delivery of therapeutic cancer vaccines and antitumor drugs to lymph and tumors *via* the intestinal lymphatic pathway. Encouragingly, yMSN high-loaded tumor-specific antigens (OVA, 11.9%) and anti-tumor drugs (Len, 28.6%) with high stability, namely Len/OVA/yMSN, efficiently co-delivered OVA and Len to their desired target sites. Moreover, yMSN concomitantly awakened the innate antitumor immunity of dendritic cells and macrophages, strengthening vaccine-induced adaptive immune responses and reversing macrophage-associated immunosuppression in the tumor microenvironment. Surprisingly, Len/OVA/yMSN treatment resulted in excellent synergistic antitumor efficacy and long-term antitumor memory in OVA-Hepa1-6-bearing mice. This high-performance nanocarrier provides a novel approach for lesion-targeting delivery of oral drugs accompanied with awakening of the innate/adaptive immunity of the lesion environment, and also represents a novel path for the oral delivery of diverse therapeutic agents targeting other lymph-mediated diseases.

*Corresponding author. Tel./fax: +86 024 43520555, Tel./fax: +86 024 43520923.
    E-mail addresses: zhangjinghai@syphu.edu.cn (Jinghai Zhang), silingwang@syphu.edu.cn (Siling Wang).

1. Introduction

Tumor-targeting delivery of antitumor agents is vital for improving the efficacy and controlling the collateral damage of cancer therapies[1,2]. Of note, recent advances have fully confirmed that the immune status of the body and even the tumor microenvironment (TME) greatly affects the curative effect of anti-tumor agents and tumor recurrence. Therefore, major efforts are underway to develop approaches that can sensitize these tumors to antitumor agents and immunity[3]. Encouragingly, recent clinical trials using immunomodulators to complement antitumor agents have once again raised the hope of a cure for many types of cancer[1,4,5]. Admittedly, intestinal lymphatic transport has proven to be an excellent pathway for delivering oral drugs for improving bioavailability by avoiding first-pass metabolism[6−10]. Recently, intestinal lymphatic pathway has focused more on the tumor-tropic and immunoregulatory features of immune cells. Abundant immune cells stored in intestinal lymphoid tissue can sense the specific signals from inflammation, tumors, and other lesions to initiate appropriate immune responses and home to these lesions[4,11]. Given this, it could be envisaged that the intestinal lymphatic pathway would be useful for tumor-targeted delivery of oral drugs or awakening of the innate/adaptive immunity of the body and the TME. In this study, a novel high-performance nanocarrier, based on the intestinal lymphatic pathway, was designed to enable the tumor-targeted delivery of oral drugs accompanied by immunity-awakening effects, further revealing the importance of intestinal lymphatic transport in tumor-target delivery and immunotherapies.

Recently, the tumor-tropic behavior of phagocytic immune cells has been recognized as a powerful potential in tumor-targeted delivery of antitumor agents[4,11]. Particularly, in addition to phagocytizing nanomedicines and delivering them to tumor sites, phagocytic immune cells can also initiate antitumor immune responses and increase the penetration of T cells and antibody therapeutics into a tumor by exploiting phagocytosis-mediated signaling[12]. With great subtlety, gut microorganisms invade into the body using the above characteristics of phagocytic immune cells[13]. As is well known, gut microorganisms survive in gastrointestinal tract (GIT) and invade into gut-associated lymphoid tissue (GALT) *via* intestinal M cells. Thereafter, they are specifically recognized and carried by endogenous dendritic cells (DCs) and macrophages and effective immunoregulation through them occurs *via* signaling by Toll-like receptors (TLRs)[14]. Gut microorganism-mediated delivery strategies provide a unique option for diverse anticancer agents and raise the possibility of dual-target delivery to lymph and tumors, as well as that of immunotherapy initiation. Recent studies have demonstrated that the yeast microcapsules can enhance the accumulation of drug molecules at diseased sites[15−19], but this method has not been used in dual-target delivery. Moreover, it faces numerous challenges, such as those involving safety concerns and quality control problems[20]. Therefore, a microorganism biomimetic nanomaterial with better biosafety and ideal physicochemical properties seems to be a more promising tool. *Saccharomyces* sp., a well-studied gut microorganism, is currently the best

candidate for biomimetic research. *Saccharomyces*-glucan, a kind of β-1,3-D-glucan from its cell wall, is stable against strong acids and digestive enzymes. It specifically recognizes C-type lectin domain family 7 member A (Dectin-1) receptors that are highly expressed on intestinal M cells, macrophages, and DCs and that triggers a series of immune responses mediated by TLRs on immunocytes to stimulate some innate and adaptive immune responses[21,22]. For example, they shift DCs from immaturity to maturity, enhancing the DCs' antigen-presenting ability and indirectly producing cytotoxic T lymphocytes (CTLs). They also reverse macrophages from protumoral M2 phenotype to antitumoral M1 phenotype, in coordination with the secretion of antitumor cytokines (such as INF-γ, IL-12, TNF-α, and NO). Made by fusing the *Saccharomyces*-glucan onto nanocores, we presume that these *Saccharomyces*-inspired nanoparticles should inherit all of the above properties of *Saccharomyces* to imbue them with dual-site specificity for oral drugs and awaken appropriate antitumor immune responses.

Mesoporous silica nanoparticles (MSNs) as carriers have uniquely suitable features for dual-site targeted delivery, including tunable size, homogeneous porosity, large storage capacity, versatile functionalization, high stability, and biocompatibility[8,23,24]. For poorly soluble molecules, MSN used ensures stable amorphous dispersion due to their excellent structural properties[25−27]. For macromolecules, MSN can allow high loading by multiple loading methods, including adsorption and covalent bonding, because of their huge superficial area and functional groups[20,28]. Thus, we here selected MSN as a core-structure for a *Saccharomyces*-inspired nanomaterial to load large amounts of insoluble Len (lenvatinib, a kind of tyrosine kinase inhibitor) in a stable amorphous form. To better verify this delivery strategy, OVA (ovalbumin, a typical model antigen) was selected as a model therapeutic cancer vaccine in this study. MSN could overcome the limitations of the poor physicochemical properties of Len and OVA for efficient co-loading. Note that high dispersal of Len in the mesoporous pores of the MSN typically poses the risk of premature leakage when delivered *in vivo*, leading to higher treatment risk and lower efficiency. Therefore, we deliberately added OVA at the openings of the nanoparticle's mesoporous pores to block such leakage. The question then became how to protect this OVA-gated Len/MSN from degradation in the GIT. *Saccharomyces*-glucan thus was used as a powerful outer coating to solve this problem.

A *Saccharomyces*-inspired nanocarrier co-loaded with Len and OVA (namely, Len/OVA/yMSN) was prepared as shown in Fig. 1. After oral administration, Len/OVA/yMSN selectively crossed intestinal M cells mediated by the Dectin-1 receptors and assembled within intestinal lymphoid follicles. Subsequently, Len/OVA/yMSN was phagocytosed and conveyed by macrophages and DCs stored in these follicles phagocytosed Len/OVA/yMSNs and conveyed them to mesenteric lymph nodes (MLNs), and then homed the nanoparticles to tumor sites. In this *in vivo* tumor-tropic journey, Len/OVA/yMSN promoted DC maturation, presenting the OVA-antigen to induce OVA-specific immune responses. In addition, macrophages were polarized into the antitumoral
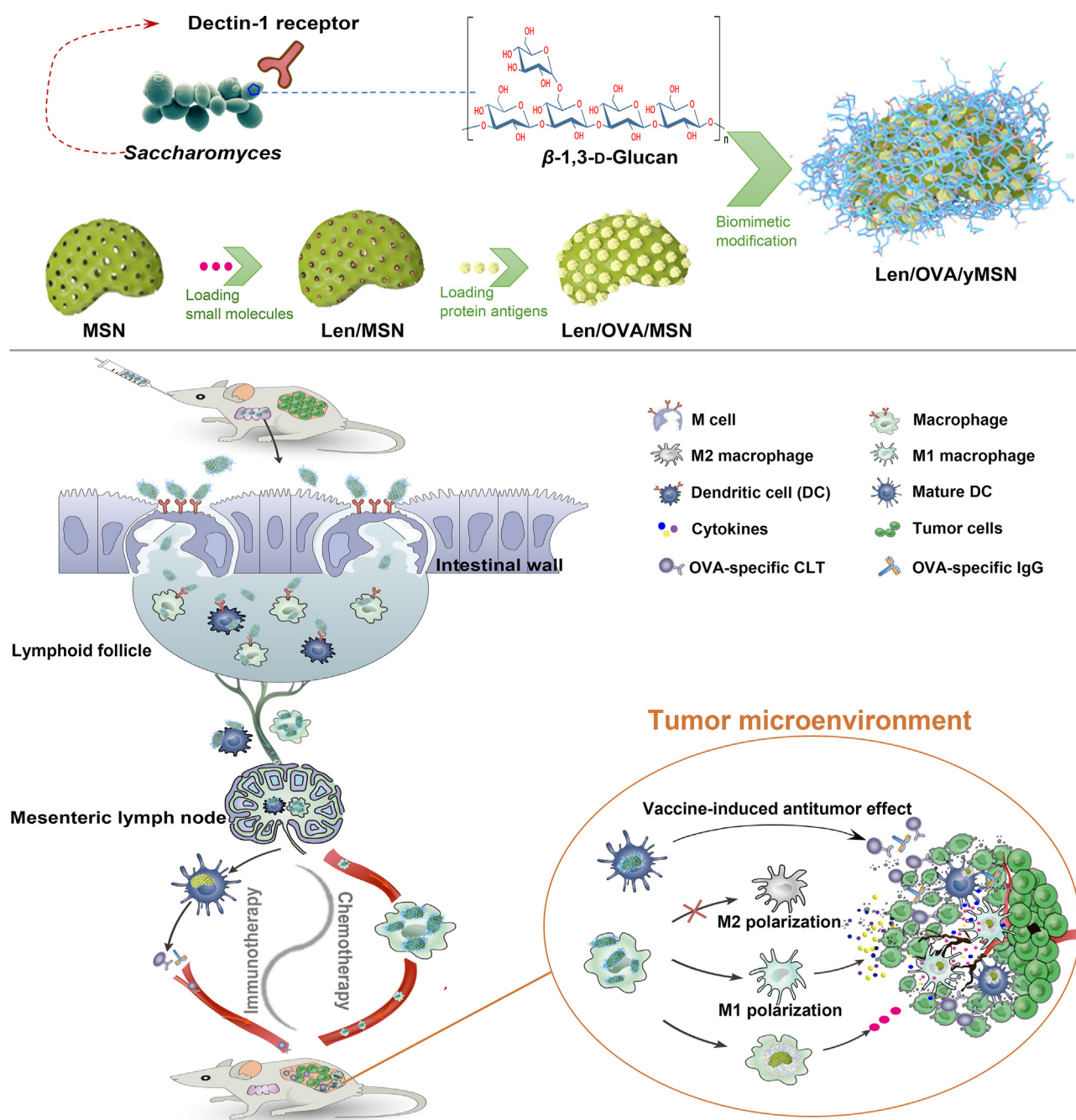
Figure 1   Schematic illustration of the design and efficacy of the Len/OVA/yMSN. After oral administration, Len/OVA/yMSN selectively crossed intestinal M cells mediated by Dectin-1 receptors and assembled within intestinal lymphoid follicles. In these follicles, macrophages and DCs phagocytosed Len/OVA/yMSNs and conveyed them to mesenteric lymph nodes (MLNs), where these nanoparticles promoted DC maturation, presenting the OVA antigen to induce OVA-specific immune responses (*i.e.*, OVA-specific CD8$^+$ T cells). Len/OVA/yMSNs also polarized macrophages toward the antitumor M1 phenotype, secreting tumor-killing cytokines, such as INF-γ, IL-12, and TNF-α. Thus, the OVA-specific CD8$^+$ T cells, M1 macrophages, and mature DCs (mDCs) carrying Len/OVA/yMSN initiated *in vivo* tumor-tropic travel. When the nanoparticles reached the tumors, Len was released from within the migrating M1 macrophages and mDCs, exerting an antiangiogenic effect and decreasing immunodepression to promote the infiltration of OVA-specific CD8$^+$ T cells into tumors.

M1 phenotype and secreted tumor-killing cytokines. When they reached the TME, Len was released from the migrating M1 macrophages and mature DCs (mDCs), exerting the excellent synergistic antitumor efficacy required for chemotherapeutics and therapeutic cancer vaccines. To our knowledge, this immunity-awakening *Saccharomyces*-inspired nanocarrier is the first designed to facilitate lymph and tumor cascade-targeted delivery of oral drugs, as well as the first to be applied to the intestinal lymphatic pathway for lesion-targeted delivery of oral drugs accompanied by immunotherapy.

2. Materials and methods

2.1. Materials

Tetraethyl orthosilicate (TEOS), 3-mercaptoprop trimethoxy silane (MPTMS, 95%), *N*-(3-dimethylaminopropyl)-*N*-ethyl carbodiimide hydrochloride (EDC), *N*-hydroxy succinimide (NHS) and OVA were obtained from Sigma−Aldrich Chemical (St. Louis, MO, USA). L-Lysine and 3-aminopropyltrieth-oxycline (APTES) were purchased from Aladdin (Shanghai, China). Fluorescein isothiocyanate (FITC) and tetraethyl rhodamine isothiocyanate (TRITC) were purchased from Fanbo Science and Technology Co., Ltd. (Beijing, China). β-1,3-D-Glucan (800−1000 KD, 85% β-1, 3-glycosidic bond) was purchased from Angel Yeast Co., Ltd. (Yichang, China). All antibodies were purchased from Thermo ebioscience Co., Ltd. (Shanghai, China). Recombinant murine GM-CSF and IL-4 were purchased from Genscript Biotech Corp (Nanjing, China). Lipopolysaccharide (LPS), lenvatinib (E7080), FBS (Bioind Fetal Bovine Serum) and DMEM (High Glucose, Gibco; Thermo Fisher Scientific, Inc.) were purchased from Meilun Biotechnology Co., Ltd. (Dalian, China). Other chemicals were all analytical as required.

2.2. Preparation of Len/OVA/yMSN

The carboxylated MSN was synthesized according to the published method[29]. The detailed procedures were described in Supporting Information. Then, 50 mg Lenvatinib (Len) was dissolved in 5 mL DMSO. Then, 5 mL prepared MSN dispersion (10 mg/mL) was added to the above Len solution, sonicated for 1 h, and stirred for 24 h at room temperature. The product was centrifuged at $6790 \times g$ and washed thoroughly with 10% DMSO to remove the adsorbed Len molecules on the surface of MSN. The Len-loaded MSN is referred to as Len/MSN.

Afterwards, the obtained Len/MSN was functionalized as shown in Supporting Information Scheme S1. First, OVA was covalently modified on the surface of Len/MSN by an amidation reaction between the amino group of the OVA structure and the carboxyl group on the surface of MSN. The procedure was as follows: 100 mg Len/MSN was dispersed into 20 mL distilled water, EDC (3 mg/mL) and NHS (2 mg/L) were added into it to activate the carboxyl groups of MSN under magnetic stirring was performed at room temperature for 1 h. Then, 50 mg OVA was added into the solution and stirred magnetically at room temperature for 24 h. After centrifugation at $6790 \times g$ for 5 min, the precipitation was collected and washed with distilled water for 3 times to obtain Len/OVA/MSN. Last, β-glucan is covalently modified on the surface of Len/OVA/MSN through the esterification reaction between the hydroxyl group of the β-glucan structure and the carboxyl group of the OVA structure on the surface of Len/OVA/MSN. The procedure was as follows: EDC (3 mg/mL) and NHS (2 mg/L) was added into 10 mL Len/OVA/MSN (10 mg/mL) dispersion to activate the carboxyl groups of OVA, stirring magnetically at room temperature for 1 h. 20 mg β-glucan was dissolved into 1 mL DMSO, and then add 5 mL distilled water, stirring magnetic force at room temperature until β-glucan is completely dissolved. The β-glucan solution was slowly added into the activated Len/OVA/MSN dispersion solution. After magnetic stirring at room temperature for 24 h, the precipitation was collected by centrifugation at $6790 \times g$ for 5 min, oscillated and washed with the distilled water for 3 times to obtain Len/OVA/yMSN.

2.3. Characterization of Len/OVA/yMSN

The morphology features were characterized by transmission electron microscope (TEM, Tecnai G2 F30, FEI, Eindhoven, Netherlands). The size distribution and zeta potentials of yMSN were determined by a Particle Size Analyzer Nicomp 380 (Particle sizing systems, USA). The Len loading capacity was determined by a Direct Ultraviolet Spectrophotometry method. Briefly, Len/OVA/yMSN was dispersed in DMSO and the concentrations of Len in the supernatants were measured by a UV−Vis spectrophotometry at 247 nm. Loading capacity was calculated by the equation as shown in Eq. (1):

$$\text{Loading capacity } (\%) = \frac{\text{Weight}_{\text{Len}}}{\text{Weight}_{\text{Len/MSN}}} \times 100 \qquad (1)$$

The amount of OVA was determined by measuring the amount of supernatant solution removed from the sample using Coomassie Brilliant Blue method, and the drug loading efficiency (%) of OVA was calculated by the equation as shown in Eq. (2):

$$\text{Loading capacity } (\%) = \frac{\text{OVA}_{\text{total}} - \text{OVA}_{\text{free}}}{\text{LMSN}_{\text{total}} + \text{OVA}_{\text{total}} - \text{OVA}_{\text{free}}} \times 100 \qquad (2)$$

The successful modifications of OVA and β-glucan were validated by color reactions, including glucose reduction of copper hydroxide and protein yellow reaction of nitric acid. The detailed procedures were described in Supporting Information. The nitrogen adsorption isotherms were measured by adsorption meter (V-Sorb 2800P, Gold APP Instrument Corporation, Beijing, China).

2.4. OVA-antigen expression and activation of BMDCs

The detailed procedures of isolation and culture of bone-marrow-derived dendritic Cells (BMDC) were described in Supporting Information. To determine the activity of OVA-antigen expression on BMDCs, BMDCs were incubated with OVA/MSN (10 mg/mL), GIT-treated OVA/MSN (10 mg/mL) yMSN (10 mg/mL), OVA/yMSN (10 mg/mL) and GIT-treated OVA/yMSN (10 mg/mL) for 24 h. Collected BMDCs, stained with APC-conjugated OVA257-264 (SIINFEKL) peptide bound to H-2Kb Monoclonal Antibody (eBioscience, CA, USA) and analyzed by flow cytometry. To determine the activity of yMSN to active BMDCs, BMDCs were incubated with MSN (10 mg/mL), Len/OVA/MSN (10 mg/mL), Len/OVA/yMSN (10 mg/mL) for 24 h. Collected BMDCs, stained with PE-conjugated anti-mouse CD80 antibody and FITC-conjugated anti-mouse CD86 antibody (eBioscience, CA, USA). The expression of costimulatory molecules CD80 and CD86 on the surface of BMDCs was detected using flow cytometry.

2.5. In vitro drug release test

In vitro release of Len: Len release behavior was examined in simulated gastric fluid (SGF, pH 1.2 with pepsin) for the first 2 h and replaced to simulated gastric fluid (SIF, pH 7.4 with trypsin) for the next 6 h. Especially, Len/OVA/yMSN (incubation) refers to Len/OVA/yMSN incubated with glucoses for 2 h to decoat the outer β-glucan coating. The concentration of Len in the release medium was quantified by UV−Vis spectroscopy at 247 nm. The cumulative release percentage of Len was calculated.

Len efflux from macrophages and BMDCs[30]: Firstly, RAW264.7 or BMDCs were incubated with Len/OVA/yMSN for 6 h in order that Len/OVA/yMSN was complete uptake into cells. Then, remove the residual Len/OVA/yMSN in the medium supernatants from macrophages or BMDCs seeded plates, and added fresh culture medium for collecting the Len efflux. The medium supernatants were collected at different time points (0, 3, 6, 12, 24, 36 and 48 h post loading) to quantify the concentrations of Len. The cumulative efflux percentage of Len was calculated as shown in Eq. (3).

$$\text{Len efflux (\%)} = \frac{\text{Len}_{sup}}{\text{Len}_{sup} + \text{Len}_{cell}} \times 100 \tag{3}$$

where Len_{sup} is the amount of Len in the supernatant; Len_{cell} is the amount of Len remained in the RAW264.7 or BMDCs.

2.6. Specific recognition and uptake of Len/OVA/yMSN by M cells

The procedure of M-cell model establishment was described in Supporting Information. FITC-labeled Len/OVA/MSN or Len/OVA/yMSN were added to the upper chamber of transwell and samples from the lower chamber were collected and analyzed by a micro-plate reader. Then, the M cell layers were washed, fixed with 4% paraformaldehyde, stained with TRITC-conjugated ulex europaeus agglutinin (UEA)-1 (to label M cells) and imaged by a Nikon C2+ laser confocal microscope (CLSM).

2.7. Specific recognition and uptake of Len/OVA/yMSN by macrophages and BMDCs

RAW264.7 cells were seeded at 1×10^5 cells per well in 12-well plates and incubated for 6 h with 20 mg of FITC-labeled Len/OVA/MSN and FITC-labeled Len/OVA/yMSN. Cells pre-incubated with Laminarin were used as control to investigate the target mechanism of Len/OVA/yMSN to BMDCs. Then, cells were collected, washed twice with PBS, the specific recognition and uptake was detected using CLSM and flow cytometry.

BMDCs were seeded at 2×10^6 cells per well in 12-well plates and incubated for 6 h with 20 mg of FITC-labeled Len/OVA/MSN and FITC-labeled Len/OVA/yMSN. Then, cells were collected, washed twice with PBS, the specific recognition and uptake was detected using flow cytometry.

2.8. Structural stability of Len/OVA/yMSN

RAW 264.7 cells were seeded at 1×10^5 cells per well into 6-well plates and incubated with fluorescent probe-labeled Len/OVA/yMSN (MSN labeled with FITC and OVA labeled with TRITC). After incubation for specified time periods, the cells were rinsed and lysed. The co-localization of TRITC-OVA and FITC-MSN was observed by CLSM and Image J was used to analyze co-localization coefficient.

2.9. Migration of Len/OVA/yMSN-loaded macrophages

RAW 264.7 cells were seeded at 2×10^6 cells per well in 6-well plates and incubated with various preparations (MSN, Len/OVA/MSN, Len/OVA/yMSN) for 4 h. Cells incubated with PBS were used as control. Collect the cells and wash with PBS. Resuspend the preparation-loaded RAW264.7 cells in the medium containing 0.5% FBS. Then, take 100 μL above cell suspension and placed on the upper chambers of transwell (6.5 mm Transwell® with 5.0 μm pore polycarbonate membrane, Corning). Subsequently, 600 μL medium containing 5 ng monocyte chemoattractant protein-1 (MCP-1, 13,14) was added into the lower chambers. After incubation for 6 h at 37 °C, the cells were fixed and stained with crystal violet. The upside membrane surface of chamber was scraped to remove the remaining cells, and the number of cells migrated to the downside surface was counted under optical microscope.

2.10. Biodistribution of Len/OVA/yMSN

Biodistribution of Len/OVA/yMSN: 100 μL Hepa1-6 cells (5×10^7 cells/mL) were subcutaneously injected at the right posterior hip of C57BL/6 mice. Experiments started when tumor size reached 100−150 mm^3. Tumor-bearing mice were randomly divided into 2 groups and were orally gavaged with Cy7-labeled Len/OVA/MSN or Cy7-labeled Len/OVA/yMSN at MSNs dose of 10 mg/kg. After 6, 12, 24 or 48 h, mice were anesthetized with 1 mL of 25% (w/v) urethane, and tissues (heart, liver, spleen, lung, kidney, MLN and tumor) were collected and stored at −80 °C until further analysis. Fluorescence images of tissues were acquired by the IVIS® Lumina Series III *in vivo* Imaging System (PerkinElmer, USA). All images we obtained were analyzed by the Living Image® 4.3.1 software provided by IVIS® Lumina Series III.

Biodistribution of Len: 100 μL Hepa1-6 cells (5×10^7 cells/mL) were subcutaneously injected at the right posterior hip of C57BL/6 mice. Experiments started when tumor size reached 100−150 mm^3. Tumor-bearing mice were randomly divided into 3 groups and were orally gavaged with Len, Len/OVA/MSN or Len/OVA/yMSN at a Len dose of 30 mg/kg. After 1, 2, 4, 6, 12, 24 or 48 h, mice were anesthetized with 1 mL of 25% (w/v) urethane, and tissues (heart, liver, spleen, lung, kidney and tumor) were collected and stored at −80 °C until further analysis. Tissue samples were thawed to room temperature, minced and homogenized to a fine paste (25%, w/v) in a tissue homogenizer (Remi, Mumbai, India) along with methanol: water (1:4) mixture. Len was extracted from tissue homogenate by adding a protein-precipitating agent, methanol in the ratio of 1:2 (v/v). Len content in tissue samples was determined by HPLC. In brief, Len was detected by a Hitachi™ HPLC system consisting of a L7100 pump and a L7420 UV−Vis tunable absorbance detector (Japan). Len was monitored at a wavelength of 247 nm.

All experimental procedures were executed according to the protocols approved by Shenyang Pharmaceutical University Animal Care and Use Committee.

2.11. Detection of cytokine secretion

RAW 264.7 cells were seeded at 2×10^6 cells per well in 6-well plates and incubated with MSN (10 μg/mL), Len/OVA/MSN (10 mg/mL) and Len/OVA/yMSN (10 mg/mL) for 24 h. Cells incubated with PBS were used as control. Cell supernatants were collected immediately and the concentrations of cytokines (NO, TNF-α, IL-12) were measured by enzyme-linked immunosorbent assay (ELISA) kits (Invitrogen, USA).

2.12. qRT-PCR array

RAW 264.7 cells were seeded at 2×10^6 cells per well in 6-well plates and incubated with MSN (10 μg/mL), Len/OVA/MSN

(10 mg/mL) and Len/OVA/yMSN (10 mg/mL) for 24 h. Cells incubated with PBS were used as control. Cells were collected for further qRT-PCR Array. Gene expression profiles were analyzed using the Human Targets of Mouse Immune-associated Signaling Related Gene qPCR Array according to the manufacturer's protocol (Wcgene Biotech, Shanghai, China). Data were analyzed using Wcgene Biotech software. Genes with fold-changes more than or less than 2.0 were considered to be of biological significance.

2.13. Western blot assay

RAW 264.7 cells were seeded at 2×10^6 cells per well in 6-well plates and incubated with MSN (10 μg/mL), Len/OVA/MSN (10 mg/mL) and Len/OVA/yMSN (10 mg/mL) for 24 h. Cells incubated with PBS were used as control. Then, RAW264.7 cells were collected, centrifuged and resuspended in RIPA buffer for immunoblotting analysis. Briefly, cell lysates in sample buffer were loaded onto a proper polyacrylamide gel and subsequently transferred onto a nitrocellulose membrane. The membranes were incubated with primary antibodies at 4 °C overnight before being blocked with 5% BSA for 1 h at 28 °C. Next, the membranes were washed and incubated with a horseradish peroxidase-conjugated secondary antibody (anti-actin antibody, anti-NF-κB p65 antibody, anti-MyD88 antibody and anti-IRAK1 antibody, all antibodies purchased from Abcam) for 1 h. Before being exposed to film and developed, the membranes were incubated with an ECL substrate kit (Abcam).

2.14. OVA-IgG determine

C57BL/6 mice were immunized *via* oral gavage with MSN, Len/OVA/MSN or Len/OVA/yMSN at the OVA dose of 200 μg/kg. The preparations were administered once a day for 14 days according to the administration schedule of anti-tumor therapy. To evaluate the serum antibody level, blood samples were collected on Days 14, 21, 28, and 35, and anti-OVA IgG levels were determined by Mouse OVA sIgG ELISA Kit (Wuhan Fine Biotech Co., Ltd.) analysis.

To investigate the OVA-specific CD8$^+$ T cell populations, mesenteric lymph nodes (MLN) of immunized mice were harvested after immunized for a flow cytometer analysis. Single-cell suspensions were prepared by using collagenase/hyaluronidase and DNase digest tumors. Then, the suspensions were lysed with ACK Lysis Buffer to remove red blood cells. Those cells were followed by staining with PE-conjugated SIINFEKL/H-2Kb peptide−MHC tetramers (Creative peptides, USA) and analyzed by flow cytometry.

2.15. In vivo antitumor efficacy

100 μL OVA expression Hepa1-6 cells (OVA-Hepa1-6 cells) (5×10^7 cells/mL) were subcutaneously injected at the right posterior hip of C57BL/6 mice. Experiments started when tumor size reached 100−150 mm^3. Tumor-bearing mice were randomly divided into 7 groups and were orally gavaged with different formulations including Len, Len/OVA/MSN, Len/OVA/yMSN, Len/yMSN, OVA/yMSN and Len/yMSN + OVA/yMSN. According to the clinical regime of Len, the dosage of formulations is at a Len dose of 10 mg/kg, QD for 14 days. Mice treated with saline were as negative control group. Len/yMSN + OVA/yMSN

group was set to evaluate the synergistic antitumor efficacy of Len/OVA/yMSN. Tumor growth was monitored by caliper at specified time points as shown in Fig. 8a. Tumor sizes were calculated by the equation as shown in Eq. (4):

$$\text{Tumor size} = a \times b^2 \times 0.5 \tag{4}$$

where a and b refer to the major and minor axes of a tumor, respectively. Then the mice were euthanized and tumors were excised for further analysis on Day 35.

Tumor rechallenge: On Day 35, the tumors of each group were excised by surgical removal from the tumor-bearing mice. Then these tumor-excised mice were then rechallenged with 1×10^6 Hepa1-6 cells or OVA-Hepa1-6 cells at the left posterior hip of these mice to further investigate the specific immune effect on antitumor therapy. The flowing tumor detection operation refers to above paragraph.

All experimental procedures were executed according to the protocols approved by Shenyang Pharmaceutical University Animal Care and Use Committee.

2.16. Immunohistochemistry analysis

The tumor tissues were fixed with 4% paraformaldehyde, and processed for immunohistochemical examination of tumor blood vessels, apoptosis (TUNEL) and immune cells. To prevent nonspecific binding of antibodies, tumor slides were blocked with the protein blocking buffer containing 4% FBS, 1% normal goat serum, and 0.01% Tween-20 in PBS for 1 h at 4 °C. For TUNEL analysis, the procedure was according to Colorimetric TUNEL Apoptosis Assay (Beyotime, China). For other detection, the slides were subsequently incubated with anti-mouse CD31 antibody (Abcam) or FITC-conjugated anti-mouse F4/80 and PE-conjugated anti-mouse CD86 or PE-conjugated anti-mouse CD206 antibodies (eBioscience, CA, USA), PE-conjugated SIINFEKL/H-2Kb peptide-MHC tetramers (Creative peptides, USA) at 4 °C. After being washed thoroughly with PBS, the slides were stained with Hoechst 33342 to identify the loci of cell nuclei. Images were captured with the microscope and CLSM. The percentage of CD31 positive area was obtained from the ratio of the CD31 positive area to the total cell area. The above experiments are provided by Servicebio Biotechnology Co., Ltd. (Wuhan, China).

2.17. Analysis of immunocytes and cytokines in tumor microenvironment

2.17.1. Tumor-associated M1/M2 macrophages
Subcutaneous tumors were harvested after treatment for a flow cytometer analysis. Single-cell suspensions were prepared by using collagenase/hyaluronidase and DNase digest tumors. Then, the suspensions were lysed with ACK Lysis Buffer to remove red blood cells. Afterwards, cells were incubated with FITC-conjugated anti-mouse F4/80 and PE-conjugated anti-mouse CD86 or PE-conjugated anti-mouse CD206 antibody (eBioscience, CA, USA) and analyzed by flow cytometry. Tumor-associated macrophages (TAMs) exist in two different phenotypes: M1 phenotype was labeled as CD86$^+$ in F4/80$^+$ and M2 phenotype was labeled as CD206$^+$ in F4/80$^+$. All the flow cytometric analysis was completed by using FlowJo software.

2.17.2. Tumor infiltrating OVA-specific CD8^{+} T cell populations

Subcutaneous tumors were harvested after treatment for a flow cytometer analysis. Single-cell suspensions were prepared by using collagenase/hyaluronidase and DNase digest tumors. Then, the suspensions were lysed with ACK Lysis Buffer to remove red blood cells. Those cells were followed by staining with PE-conjugated SIINFEKL/H-2Kb peptide−MHC tetramers (Creative peptides, USA) and analyzed by flow cytometry.

2.17.3. Cytokines levels

Subcutaneous tumors were harvested after treatment for a cytokines analysis. Tumor homogenate was prepared immediately and the concentrations of cytokines (NO, TNF-α, IL-12) were measured by enzyme-linked immunosorbent assay (ELISA) kits (Invitrogen, USA).

2.18. Statistical analyses

Statistical analyses were performed by Student's *t*-test, one-way analysis of variance, two-way analysis of variance or unpaired *t*-test. All statistical analyses were done with GraphPad Prism 6.

3. Results and discussion

3.1. Characterization and in vitro properties of Len/OVA/yMSN

Len/OVA/yMSN was prepared as shown in Scheme S1. TEM was used to assess the morphology of MSN, Len/OVA/MSN, and Len/OVA/yMSN (Fig. 2A). Monodisperse Len/OVA/yMSN with a diameter of 299.6 ± 10.7 nm and a zeta potential of −19.8 ± 0.7 mV (Fig. 2B) was obtained after coating with 5.15% *Saccharomyces*-glucan on the surface of Len/OVA/MSN, and this Len/OVA/yMSN allowed a high load of Len and OVA up to 28.6% (286 mg Len/1 g Len/OVA/yMSN) and 11.9% (119 mg OVA/1 g Len/OVA/yMSN), respectively (Fig. 2C). Besides, OVA/yMSN and Len/yMSN were also prepared as control formulations and the characterization results were shown in Supporting Information Fig. S1. Furthermore, we validated the successful modification of *Saccharomyces*-glucan to the surface of Len/OVA/MSN by the characteristic color reaction of glucose, based on the generation of orange cuprous oxide (Fig. 2D).

After successfully preparing Len/OVA/yMSNs, their essential *in vitro* properties were investigated in the following study. First, the structural integrity of Len/OVA/yMSNs in the GIT (evaluated in simulated gastroenteric fluid) was assessed and is shown in Fig. 2E. TEM images revealed that the *Saccharomyces*-glucan layer was still observable after an 8 h incubation in the GIT. Additionally, after 24 h, only fragments of the *Saccharomyces*-glucan layer were left on the surface of the Len/OVA/yMSNs. Usually, such a slow degradation rate could ensure that the Len/OVA/yMSNs taken up by the intestine are intact after oral administration 7. We next investigated the protective effect of the *Saccharomyces*-glucan layers on OVA bioactivity in the GIT. As shown in Fig. 2F, the characteristic color reaction of protein and the results of sodium dodecyl sulfate polyacrylamide gel electrophoresis (SDS-PAGE) showed that 69.25% of the OVA remained on OVA/yMSNs after incubation in simulated gastrointestinal fluid (post-GIT), compared with non-treated OVA/yMSNs (pre-GIT), while almost no OVA was left on OVA/MSNs. This demonstrated the ability of the *Saccharomyces*-glucan layer to protect against OVA degradation in the GIT. The antigenicity of

OVA was further assessed by detection of the level of antigenic peptide-major histocompatibility complex class I (SIINFEKL-MHC-I) complexes in BMDCs. As shown in Fig. 2G, GIT-treated OVA/yMSNs generated unimpaired levels (9.46%) of SIINFEKL-MHC-I complexes compared with non-treated OVA/yMSN (8.26%), whereas GIT-treated OVA/MSNs significantly reduced the levels (3.43%) of SIINFEKL-MHC-I complexes compared with non-treated OVA/MSNs (1.53%), further indicating the protective effect of *Saccharomyces*-glucan coating on the surface of OVA/MSNs. Amazingly, non-treated OVA/yMSNs induced an approximately 2.76-fold higher antigen-presenting response compared with non-treated OVA/MSNs in BMDCs, implying a stimulation effect on innate immune response of BMDCs by yMSN. Strictly speaking, innate immune stimulation is essential to achieving a robust antigen-specific T-cell response[31].

Additionally, the microstructures of these MSNs, a key factor in drug loading and releasing, was assessed *via* BET nitrogen adsorption−desorption isotherms. A cumulative pore volume (V_t) of 1.41 cm^3/g, a surface area (S_{BET}) of 811.57 m^2/g (Supporting Information Fig. S2), and an average pore size of approximately 6.67 nm (Supporting Information Table S1) indicated that these MSNs had sufficient properties for abundant loading, stable dispersion, and rapid release of drugs. However, modifying MSNs with OVA on their surfaces noticeably reduced their surface area (536.31 m^2/g), indicating that the opening mesoporous pores of MSNs were blocked to prevent premature drug leakage when delivered *in vivo*. A further sharp reduction in the surface area (106.17 m^2/g) of OVA/yMSNs implied the formation of an outermost protective layer of *Saccharomyces*-glucan, which ensured the structural stability of Len/OVA/yMSNs when across the GIT. Interestingly, this outermost protective layer was removed from the surface of OVA/MSNs by lysozyme (abundant in macrophages), re-exposing the mesoporous pores (the surface area up to 761.53 m^2/g) to release the drug loaded in mesoporous pores.

For the oral delivery of insoluble small-drug molecules, premature leakage during *in vivo* delivery and difficult release at lesions always leads to higher risk and lower efficiency. Our Len/OVA/yMSNs held promise for preventing the premature leakage of drug when across the GIT. An *in vitro* release test was performed to show the release behavior of Len trapped in Len/OVA/yMSNs in simulated gastric fluid (SGF, pH 1.2) and with simulated intestinal fluid (SIF, pH 7.4). The Len release curves are presented in Fig. 2H. Poorly soluble Len displayed a very slow Len release whether in SGF (3.60% for 2 h) or in SIF (16.33% for 6 h). Very different Len release curves were found in other Len formulations. Fast and complete Len release from Len/MSNs in both SGF (47.53% for 2 h) and SIF (86.69% for 6 h) was seen mainly because of the high dispersion of insoluble Len by mesoporous channels in MSNs. A total of 79.03% of the Len was rapidly released within 8 h from Len/OVA/MSNs, indicating that only OVA modified on the surface of MSNs failed to show the desired blocking effect of Len dispersed in the pores of MSNs. However, there was a significantly slower Len release from Len/OVA/yMSNs, reaching only 7.53% within 2 h in SGF and maintaining a steady, slow release over 8 h up to 32.69%. Most notably, when we pre-treated Len/OVA/yMSNs with glucanase (to hydrolyze the *Saccharomyces*-glucan coating) , almost 73.36% of the Len was rapidly released within 8 h from Len/OVA/yMSNs (incubation). Taken together, the double block effects of *Saccharomyces*-glucan and OVA might prevent earlier release of Len in
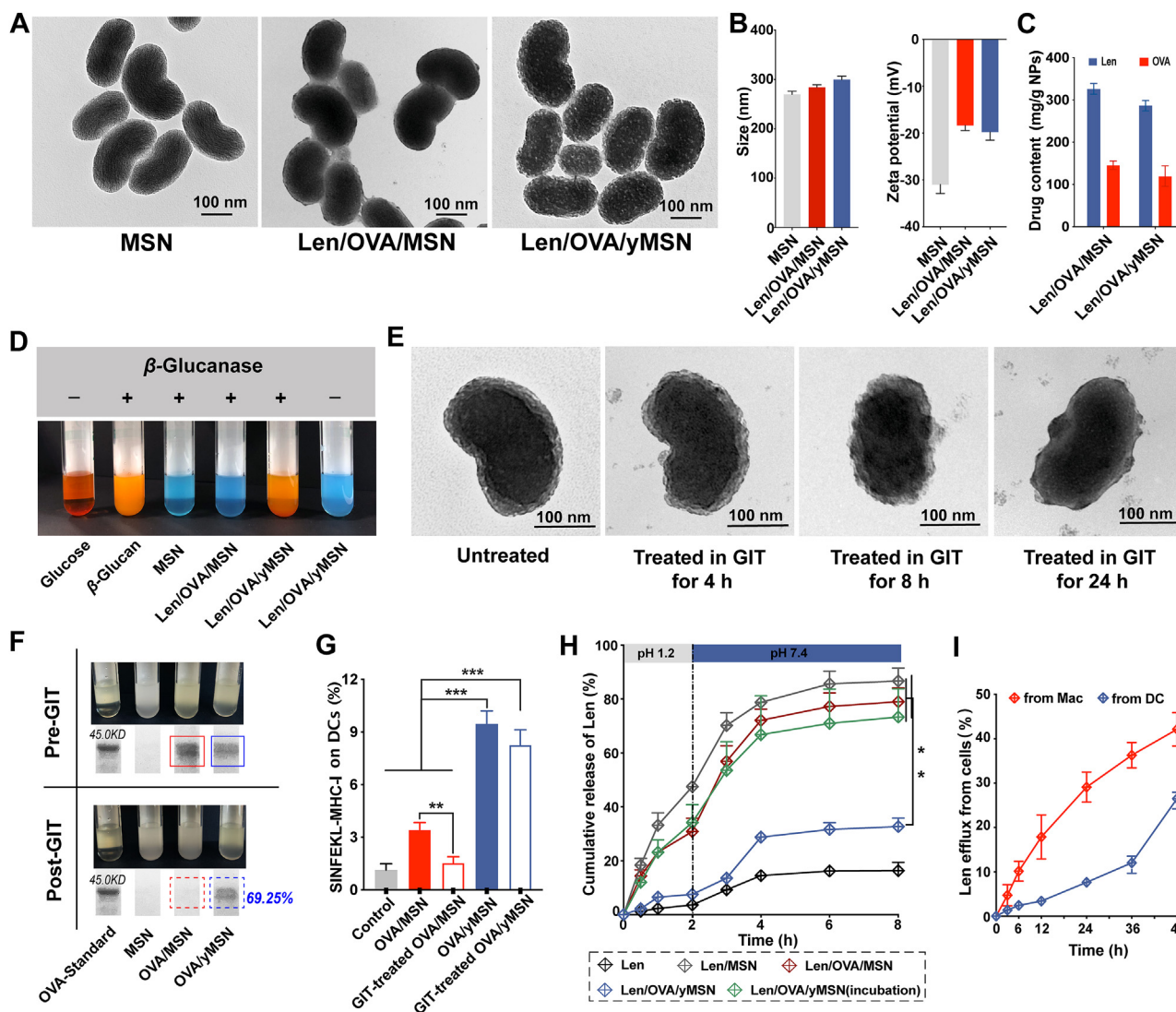
Figure 2 Characterization and *in vitro* properties studies of Len/OVA/yMSN. (A) TEM images of MSNs, Len/OVA/MSNs and Len/OVA/yMSNs. (B) Particle size and surface zeta potential of MSNs, Len/OVA/MSNs, and Len/OVA/yMSNs ($n = 3$). (C) Loading capacities of Len and OVA ($n = 3$). (D) Glucose reduction reaction with copper hydroxide, indicating successful modification with *Saccharomyces*-glucan. (E) Integrity of Len/OVA/yMSNs in the GIT. (F) Qualitative and quantitative analysis of OVA on the surface of MSNs using protein yellow reaction and SDS-PAGE. (G) BMDCs presenting antigenic SIINFEKL peptide on the MHC molecule as analyzed by FCM ($n = 3$). (H) *In vitro* Len release from different Len formulations in SGF and SIF ($n = 5$). (I) Len efflux from macrophages and DCs ($n = 5$). All of the data are presented as the mean ± SD. **$P < 0.01$; ***$P < 0.001$.

the GIT, retaining more of this drug to be absorbed by and to accumulate in tumors. We then analyzed the Len efflux in macrophages and DCs. As shown in Fig. 2I, a time-dependent increase in Len was observed in both cell culture supernatants, which released near 42.12% of the Len in macrophages and 26.47% of it in DCs within 48 h.

3.2. Targeting abilities of Len/OVA/yMSNs

To precisely target to tumors *via* the oral route in the manner of *Saccharomyces*, specific recognition of Len/OVA/yMSNs by intestinal M cells and macrophages is necessary. First, an M-cell model was established to explore the specific recognition between the Len/OVA/yMSNs and M cells. Caco-2 and Raji B cell monolayers were formed on eight-well Transwell culture plates according to a previously published method (Fig. 3A-middle)[32]. A

greater colocalization of Len/OVA/yMSNs on M cells (Pearsons' coefficient, 0.895) was observed (Fig. 3A-left) when compared with Len/OVA/MSNs (Pearsons coefficient, 0.571), and the transportation amount of Len/OVA/yMSNs through our M-cell model was approximately 1.87 times higher than that of Len/OVA/MSNs (Fig. 3A-right). Furthermore, we used laminarin, a potent competitive inhibitor of the Dectin-1 receptors, to explore the mechanism of the specific recognition between Len/OVA/yMSNs and M cells. Laminarin significantly decreased the amount of Len/OVA/yMSNs transported through monolayer M cells, indicating that such transport of Len/OVA/yMSNs was mediated by the Dectin-1 receptors on M cells. These results validated that our *Saccharomyces*-glucan coating could significantly promote the specific transport of Len/OVA/yMSNs through M-cells.

Special recognition between Len/OVA/yMSNs and macrophages is also vital to subsequent cell-mediated tumor-tracking
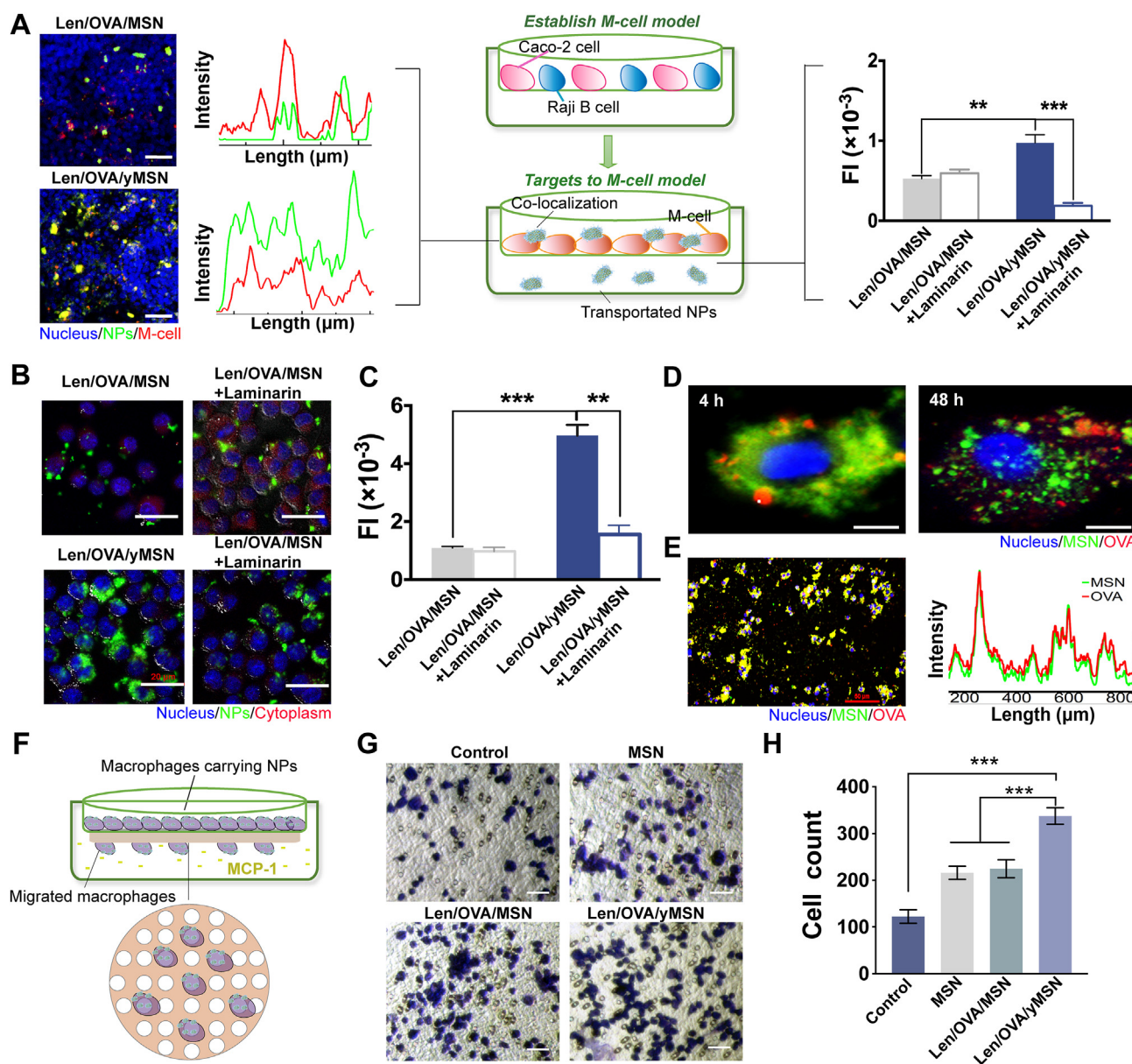
Figure 3 *In vitro* targeting abilities. (A) Left: co-localization of nanoparticles with M cells with the corresponding co-localization analysis (co-localization curves); scale bar = 50 μm. Middle: schematic diagram of M-cell model establishment and co-localization. Right: the transport amount of nanoparticles transported through the M-cell monolayer (*n* = 3). (B) CLSM images of the specific uptake of Len/OVA/yMSN uptake by RAW 264.7 cells; scale bar = 20 μm. (C) FCM analysis of the specific uptake of Len/OVA/yMSN uptake by RAW 264.7 cells (*n* = 3). (D) CLSM images of the co-localization of OVA and MSNs in macrophages at 4 h and 48 h; scale bar = 10 μm. (E) CLSM images of OVA and MSN co-localization in macrophages at 24 h with corresponding co-localization analysis; scale bar = 50 μm. (F) Schematic diagram of macrophages carrying Len/OVA/yMSNs. (G) Representative high-power field (HPF) images of migrated macrophages; scale bar = 100 μm. (H) Quantitative analysis of migrated macrophages (*n* = 3). All of the data are presented as the mean ± SD. **$P < 0.01$; ***$P < 0.001$.

delivery *in vivo*. Therefore, we explored the specific recognition between Len/OVA/yMSNs and macrophages. CLSM images showed a higher internalization of Len/OVA/yMSNs than of Len/OVA/MSNs by macrophages (Fig. 3B and Supporting Information Fig. S3) compared with Len/OVA/MSNs. Notably, when we added laminarin before macrophage uptake, a completely different internalization pattern appeared: internalization of Len/OVA/yMSNs by macrophages was reduced, but that of Len/OVA/MSNs was almost unchanged. Flow cytometry (FCM) further showed

that macrophagic internalization of Len/OVA/yMSNs was 2.11-fold higher than that of Len/OVA/MSNs, a significant difference, and that laminarin reduced the former by 75%, which was also statistically significant (Fig. 3C). Taken together, these results indicated that *Saccharomyces*-glucan coating fully enabled specific macrophagic internalization of Len/OVA/yMSNs mediated by Dectin-1 receptors[33−35].

We then explored the integrity of Len/OVA/yMSNs in macrophages. In our study, Len/OVA/yMSNs stayed as intact for the

first 4 h in macrophages but they were almost completely disintegrated at 48 h in macrophages (Fig. 3D). Intact Len/OVA/yMSNs in macrophages could be observed when they were inside macrophages for 24 h, as is shown in Fig. 3E, which represents a sufficiently long time for the *in vivo* delivery from intestinal lymphatic follicles to distant tumors. Additionally, the safety and migratability of macrophages after carrying Len/OVA/yMSNs were assessed. Len/OVA/yMSNs exhibited no cytotoxicity to macrophages (Supporting Information Fig. S4). Interestingly, we found that macrophages carrying MSN or Len/OVA/MSN showed equivalent enhanced migratability compared with macrophages carrying nothing (Fig. 3F−H). Accumulating results indicate that RAW264.7 cells after silicon nanoparticles loading were polarized and secreted various cytokines, cytokines, including IL-1β, IL-6, IL-12, TNF-α, and IL-10[30,36]. This is probably the main reason for the enhanced migration of macrophages carrying MSN or Len/OVA/MSN. It pays more attention that macrophages carrying Len/OVA/yMSNs revealed the highest migratability compared with macrophages carrying nothing, MSNs or Len/OVA/MSNs, mainly due to *Saccharomyces*-glucan's stimulatory effects on the macrophages[21,22]. These results highlighted the possibility of subsequent macrophage-mediated tumor-tracking delivery *in vivo*.

3.3. Dual-target delivery in vivo of Len/OVA/yMSN similar to that of Saccharomyces

Next, the *in vivo* lymph-targeting delivery of Len/OVA/yMSNs was explored step by step. First of all, *ex vivo* fluorescence images displayed greater specific accumulation of Len/OVA/yMSNs than of Len/OVA/MSNs in Peyer's patches compared with that of Len/OVA/MSNs (Fig. 4A), and many more fluorescence signals for Len/OVA/yMSNs were further observed in a Peyer's patch section 6 h after oral administration than that treated with Len/OVA/MSNs (Fig. 4B). This further demonstrated the accumulation tendency of Len/OVA/yMSNs in Peyer's patches during intestinal absorption. Remarkably, a higher colocalization of Len/OVA/yMSNs with intestinal M cells was shown in CLSM images compared with that of Len/OVA/MSNs (Fig. 4C), suggesting that these Len/OVA/yMSNs entered the intestinal lamina propria mostly *via* M cells. Whether these Len/OVA/yMSNs could be taken up by macrophages in lymphoid follicles or not should directly affect subsequent tumor-targeting delivery. CLSM images of lymphoid follicles affirmed the obvious existence of Len/OVA/yMSNs in macrophages (Fig. 4D), in which the amount of Len/OVA/yMSNs was 5.5-fold higher than that of Len/OVA/MSN in macrophages based on FCM analysis (Fig. 4E). We then explored the targeting ability of Len/OVA/yMSNs to target MLN *in vivo*. 6 h after oral administration, stronger fluorescence signals for Len/OVA/yMSNs were observed than for Len/OVA/MSNs in MLNs (Fig. 4F). Likewise, CLSM images of MLN cryosections affirmed the existence of Len/OVA/yMSNs in macrophages in particular (Fig. 4G), and the amount of Len/OVA/yMSNs in these macrophages was 1.9-fold higher than that of Len/OVA/MSNs (Fig. 4H). This suggested that the macrophages stored in intestinal lymphoid follicles phagocytosed the Len/OVA/yMSNs and conveyed them to MLNs. Surprisingly, Len/OVA/yMSNs also displayed a significantly higher co-localization with DCs in MLNs than Len/OVA/MSNs (Fig. 4I and J) due to the specific recognition of *Saccharomyces*-glucan by the Dectin-1 receptor, which is highly expressed on DCs[34,37]. Therefore, Len/OVA/yMSNs could be potential nanocarriers of oral vaccines for effective delivery of antigens to APCs.

After validating that Len/OVA/yMSNs could target to the MLN *via* phagocytosis and conveyance by macrophages and DCs stored in intestinal lymphoid follicles after oral administration, we next evaluated their targeting ability to tumors *in vivo* using tumor-bearing C57BL/6 mice. First, we investigated the tumor accumulation and retention of Cy7-labeled Len/OVA/yMSNs after oral gavage into mice bearing subcutaneous Hepa1-6 tumors. Cy7-labeled Len/OVA/MSNs were also orally gavaged as a control group. We monitored the Cy7 signal in mice with an IVIS system over a period of 48 h following oral administration of these formulations. Cy7-labeled Len/OVA/yMSNs showed a greater fluorescence intensity within tumors than Cy7-labeled Len/OVA/MSNs at 24 h (Fig. 5A). Forty-eight hours later, a gradual increase of Cy7-labeled Len/OVA/yMSN signals was observed compared with a gradual disappearance of Cy7-labeled Len/OVA/MSN signal, indicating that Len/OVA/yMSNs had a selectively accumulating tendency at tumor sites. As demonstrated by *ex vivo* images at 48 h (Fig. 5B), Cy7-labeled Len/OVA/yMSNs exhibited stronger signals in the tumor, liver, and spleen when compared with Cy7-labeled Len/OVA/MSNs. To investigate whether Cy7-labeled Len/OVA/yMSNs were conveyed by macrophages to tumors, we further analyzed tumor cryosections by CLSM. Macrophages were specifically labeled with PE-conjugated anti-mouse F4/80 antibody. The results affirmed the existence of Cy7-labeled Len/OVA/yMSNs in macrophages, while almost no fluorescence signals for Cy7-labeled Len/OVA/MSNs were observed in macrophages (Fig. 5C). Complementary to this, FCM showed that Cy7-labeled Len/OVA/yMSNs exhibited a much higher percentage (53.1%) in macrophages in tumors than Cy7-labeled Len/OVA/MSNs (1.3%) (Fig. 5D). These results fully demonstrated that Len/OVA/yMSNs could be selectively conveyed to tumors by macrophages in a tumor-homing manner[4,11], owing to the specific recognition of the *Saccharomyces*-glucan coating on the surface of Len/OVA/MSNs to Dectin-1 receptors that are highly expressed on macrophages[34,37]. Consistently, orally delivered yeast capsules are demonstrated mainly distributed in monocytes after they enter the bloodstream, followed by transportation to the diseased sites by monocytes/macrophages[15,16,38].

We next evaluated the accumulation and retention of Len in tumors delivered by Len/OVA/yMSNs after oral gavage of tumor-bearing C57BL/6 mice (Fig. 5E). In the first 6 h, both Len administered alone and Len/OVA/MSNs yielded higher concentrations of Len than Len/OVA/yMSNs, due to both the former primarily being transported into systemic circulation *via* the traditional intestinal-absorption pathway, with time to peak at 4 h. After 6 h, Len/OVA/yMSNs yielded a significantly higher overall level of Len within mouse tumors than Len/OVA/MSNs or Len alone. Until 48 h, we observed 12.37-fold higher levels of Len within tumors from Len/OVA/yMSNs than from Len/OVA/MSNs. These results all indicated that Len/OVA/yMSNs increased both accumulation and retention of Len in tumors after oral administration. To evaluate the tumor-targeting ability of Len/OVA/yMSNs across all main organs, we calculated percentages of Len distributed in the heart, liver, spleen, lung, kidney, and tumors at all time points. As shown in Fig. 5F and Supporting Information Table S3, orally administered Len/OVA/yMSNs yielded the highest percentage of Len in organs at 24 h (5.71%) and 48 h (13.6%), compared with the peak percentages of Len alone (4.52%) and of Len/OVA/MSNs (2.87%). Such changes in Len biodistribution indicated that Len/OVA/yMSNs have the potential to deliver drugs precisely to tumors with less off-target toxicity *via* oral routes. All of these data further suggested that coating the
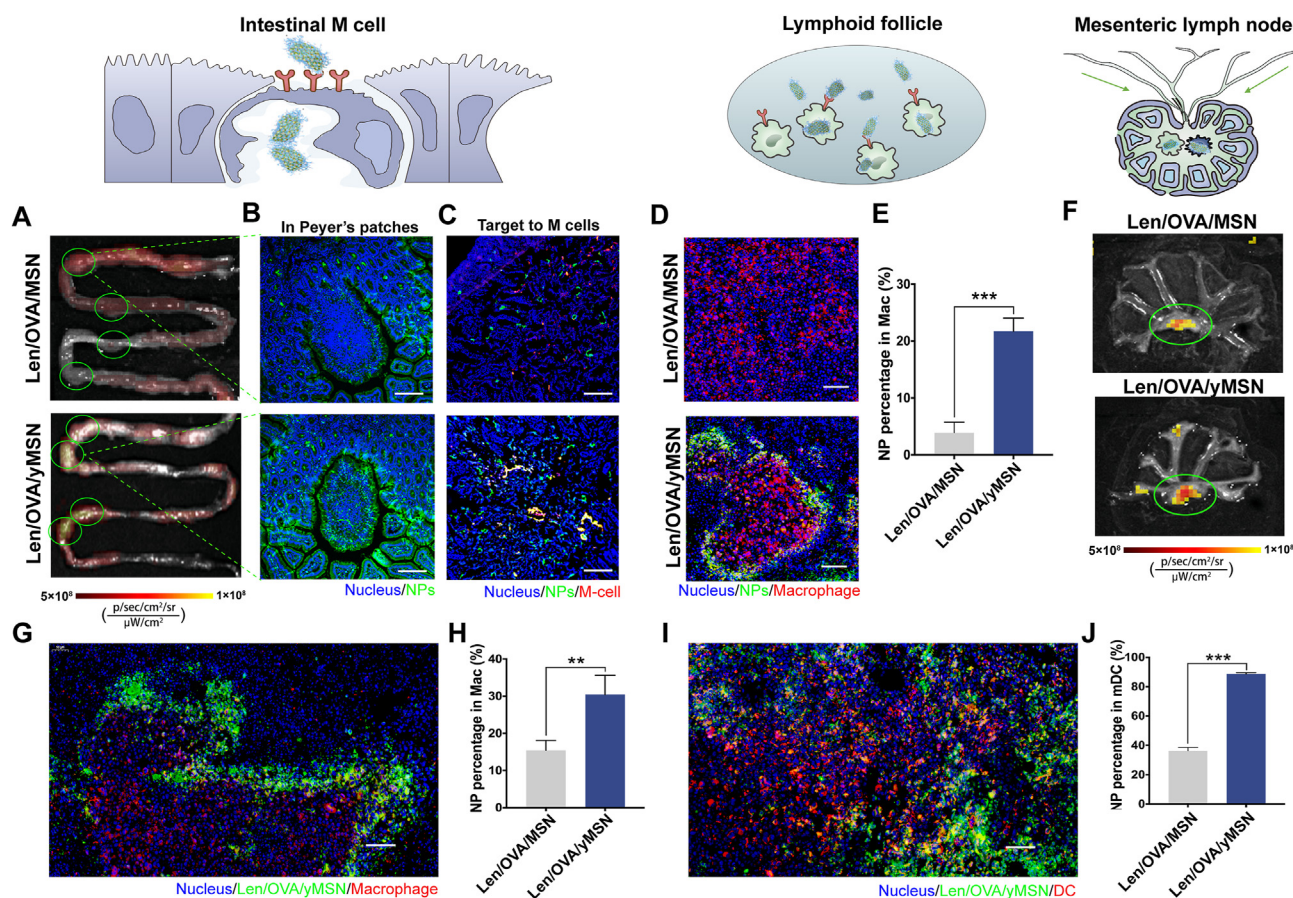
Figure 4 *In vivo* lymph-targeting delivery of Len/OVA/yMSNs. (A) Localization of Len/OVA/MSNs or Len/OVA/yMSNs in Peyer's patches 6 h after oral administration by *ex vivo* fluorescence imaging (green circles show Peyer's' patches); (B) Distribution of Len/OVA/MSNs or Len/OVA/yMSNs (green) in Peyer's' patches by CLSM; scale bar = 200 μm. (C) Co-localization of Len/OVA/MSNs or Len/OVA/yMSNs (green) with intestinal M-cells (red) by CLSM; scale bar = 200 μm. (D) Co-localization of Len/OVA/MSNs or Len/OVA/yMSNs (green) with macrophages (red) in lymphoid follicle sections by immunofluorescence; scale bar = 100 μm. (E) Quantification of nanoparticles in macrophages in lymphoid follicles after oral administration by FCM (*n* = 3). (F) Localization of Len/OVA/MSNs or Len/OVA/yMSNs in the mesenteric lymph node by *ex vivo* fluorescence imaging. (G−J) Co-localization of Len/OVA/yMSNs (green) with macrophages (red) or DCs (red) in MLNs by immunofluorescence imaging; scale bar = 100 μm; and quantification of nanoparticles in macrophages or CD11c$^+$ DCs in mesenteric lymph nodes after oral administration by FCM (*n* = 3). All of the data are presented as the mean ± SD. **$P < 0.01$; ***$P < 0.001$.

surfaces of MSNs with *Saccharomyces*-glucan could change their original delivery route *via* a unique mechanism similar to that of *Saccharomyces*.

Taken together, these findings showed that Len/OVA/yMSNs demonstrated tremendous efficacy in being recognized, which ensured their entry into a subsequent intricate process of immunocyte-mediated lymph-targeting and tumor-homing transportation *in vivo*.

3.4. Awakening of antitumor immunity by Len/OVA/yMSNs

In addition to the outstanding function of cascade targeted delivery to lymph and tumors, Len/OVA/yMSNs also were found to modulate the regulation of innate immune responses due to the immunogenicity of *Saccharomyces*-glucan. It is well known that stimulating innate immune cells can provoke antitumor effects[39]. Usually, tumor recruiting macrophages, especially those of the M1 phenotype, are a classical activated kind of macrophage with antitumor immune responses to secreting cytokines that function to kill tumors in the initial period after infection begins[40]. After a

period of tumor domestication, TAMs transform into the M2 phenotype, which exert pro-tumorigenic activities, including tumor invasion, metastasis, and angiogenesis[41,42]. Thus, altering the tumor microenvironment by reversing adverse polarization of TAMs is critical for immunotherapy. A series of experiments were thus conducted to assess the effects of Len/OVA/yMSNs on the regulation of innate immune responses. Surprisingly, a significant increase in antitumoral M1 macrophages and a reduction of pro-tumoral M2 macrophages were promoted by Len/OVA/yMSNs (Fig. 6A), accompanied by the release of a large number of antitumor cytokines (NO, IL-12, and TNF-α) over the other three groups, demonstrating the effective activation of macrophages after cellular internalization of Len/OVA/yMSNs. As a result, a strong cell-killing effect (approximately 90%) of macrophages carrying yMSNs on Hepa1-6 tumor cells was exhibited. Altogether, we concluded that Len/OVA/yMSNs were able to induce a series of antitumor responses in macrophages (Fig. 6B). Compared with the data obtained from the Len/OVA/MSN group, we reasonably speculated such strong immune regulation effects of Len/OVA/yMSNs were based on the *Saccharomyces*-glucan
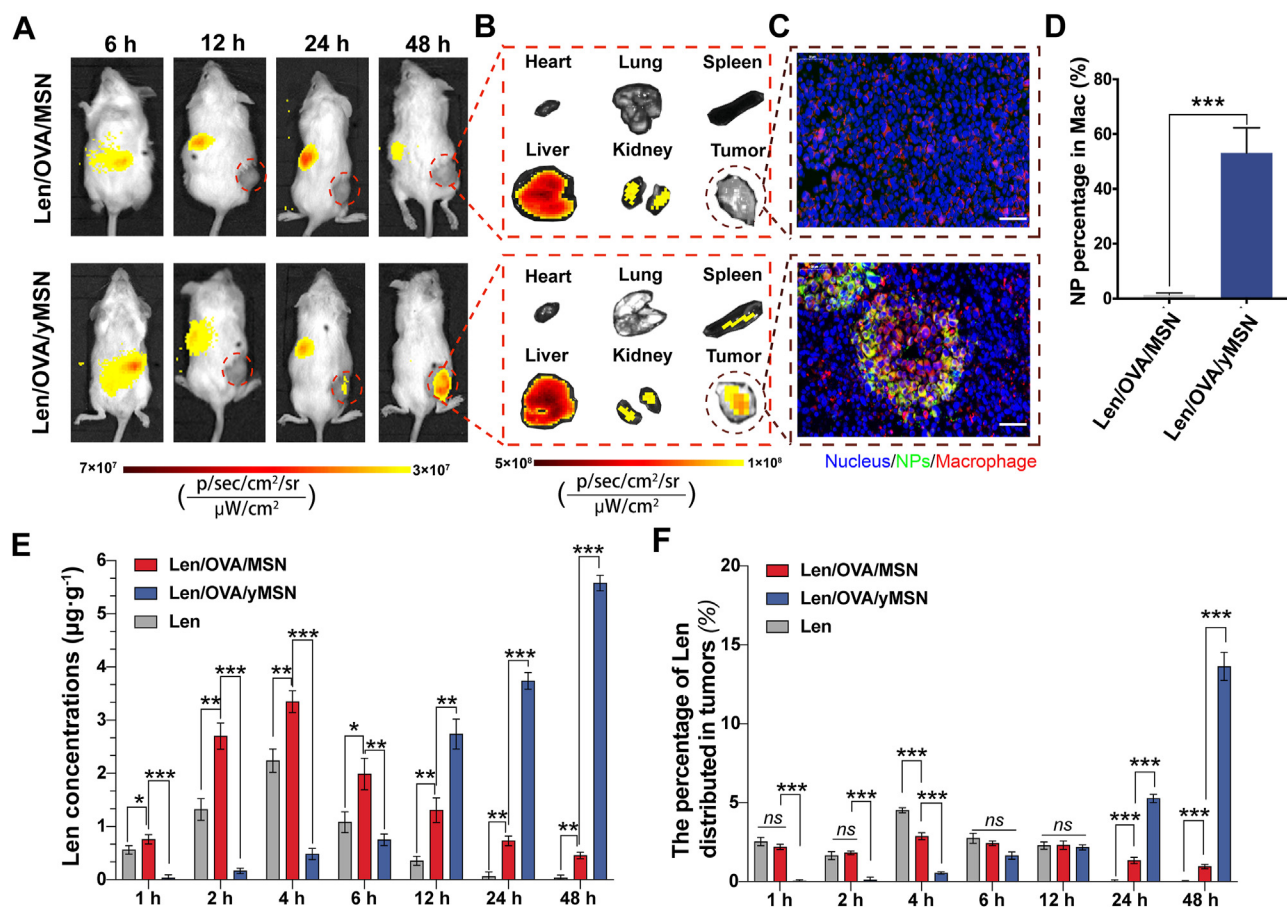
Figure 5 *In vivo* tumor-targeting delivery of Len/OVA/yMSNs. Biodistribution of nanoparticles in mice by *in vivo* (A) and *ex vivo* (B) fluorescence imaging; scale bar = 50 μm. (C) Co-localization of Cy7-labeled Len/OVA/MSNs or Cy7-labeled Len/OVA/yMSNs (green) with macrophages (red) in tumor sections by immunofluorescence imaging; scale bar = 50 μm. (D) Quantification of nanoparticles in macrophages in tumors after oral administration of nanoparticles by FCM ($n = 3$). (E) Concentrations of Len in tumors ($n = 3$). (F) Percentages of Len distributed to tumors in all main organs ($n = 5$). All of the data are presented as the mean ± SD. *$P < 0.05$; **$P < 0.01$; ***$P < 0.001$. *ns*, not significance.

coating, which could act on several immune receptors, including Dectin-1 and TLRs, and stimulate a group of immune cells, including macrophages, DCs, neutrophils, monocytes, and natural killer cells.

We then explored the mechanism by which Len/OVA/yMSNs stimulated antitumor immune responses, analyzing key genes and proteins according to the main immune-related signaling pathways in macrophages (Fig. 6C), key genes and proteins were analyzed in our study. As highlighted on the heatmap (Fig. 6D), the significant genes were mainly involved in TLR 2/4-mediated immune responses (Fig. 6E, Supporting Information Fig. S6 and Table S2) and reflected preliminary signaling pathways activated by Len/OVA/yMSNs in macrophages as shown in Fig. 6C. Significant upregulations of some major proteins (*i.e.*, MyD88, IRAK1, and NF-κB) (Fig. 6F) involved in the signaling pathways[43] were further strengthened by the immune activation effect of Len/OVA/yMSNs in macrophages. These changes cumulatively triggered intracellular signaling that induced macrophages to boost their antitumor immune responses. In conclusion, Len/OVA/yMSNs constitute an immunomodulatory delivery system that holds huge potential for controlling macrophage activation that functions *via* the TLR-2/4 signaling pathway.

As is well known, macrophages settling down in tumors usually yield to the local immunosuppressive condition of the TME and convert from the antitumor M1 phenotype to the protumor M2 phenotype, leading to weakened immune response[44]. Our results demonstrated that the yMSNs carried by macrophages could not only activated these macrophages more strongly but also lent them better resistance against M2 modification within tumors, which could be beneficial *in vivo* antitumor therapy.

Additionally, Len/OVA/yMSNs were also designed to deliver OVA as a therapeutic cancer vaccine to fight cancer *via* a robust adaptive immunotherapy—antigen-specific T-cells and antibodies (Fig. 7A). Consistent with the previous result in this study, Len/OVA/yMSNs displayed a significantly higher colocalization in DCs when compared with Len/OVA/MSNs (Fig. 7B), owing to the specific recognition of *Saccharomyces*-glucan by the Dectin-1 receptor that is highly expressed on DCs[34,37]. Also, Len/OVA/yMSNs stimulated naïve BMDCs to generate CD11c⁺CD80⁺CD86⁺ cell populations at the high percentage of 43.0% compared with Len/OVA/MSNs (10.6%) (Fig. 7C), implying that Len/OVA/yMSNs could effectively promote DCs maturation. Notably, MSN showed the strongest stimulating effect due to the markable additional adjuvant effects of sialic nanospheres[45−47]. Mature DCs
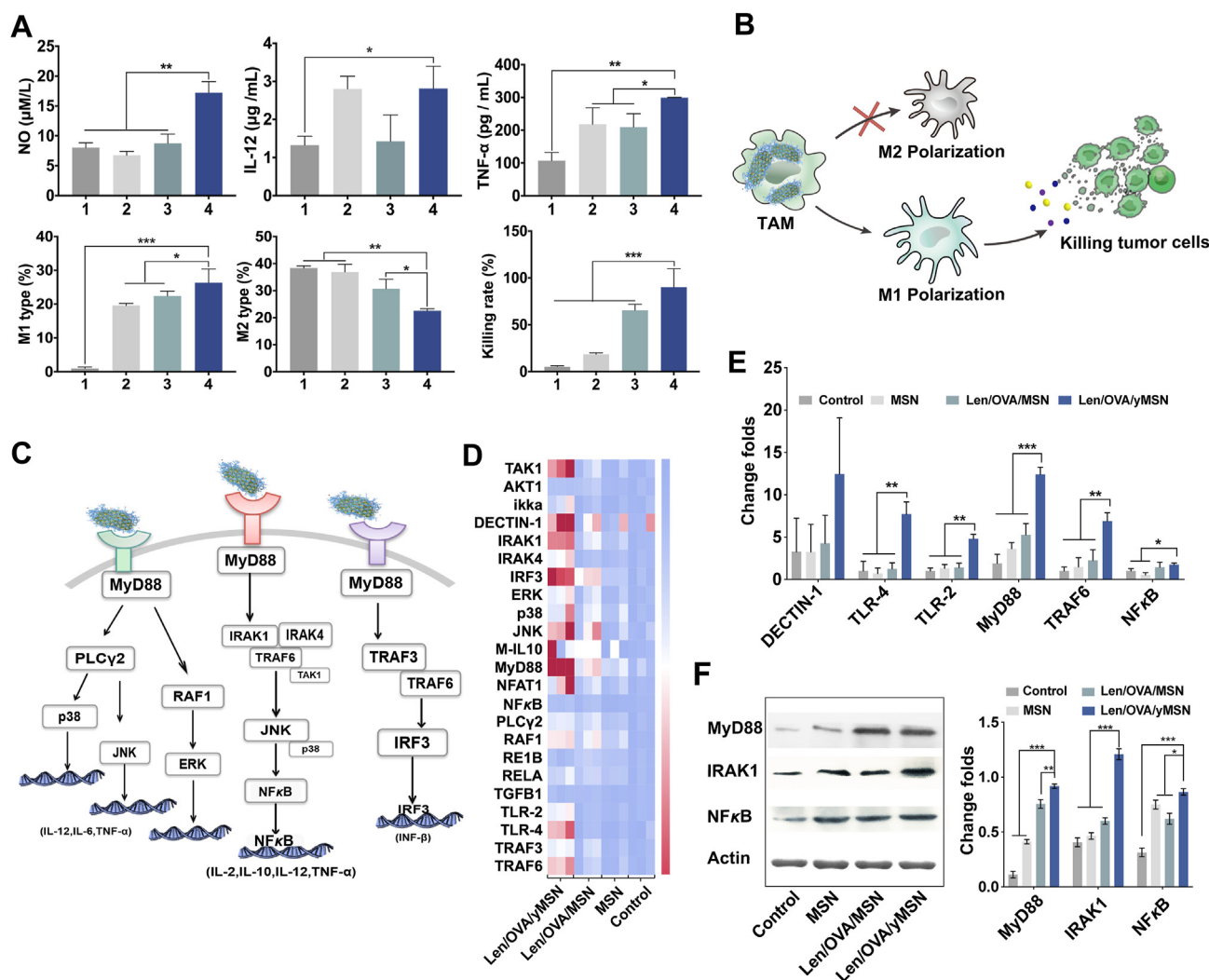
Figure 6 Innate immunomodulatory mechanism and efficacy of the Len/OVA/yMSN to macrophages. (A) Relative quantification of the ratio of M1-type macrophages and M2-type macrophages induced by yMSNs, secretion of cytokines (NO, IL-12 and TNF-α), and the cell-killing rate of macrophages carrying Len/OVA/yMSN to Hepa1-6 tumor cells ($n = 3$). (1. Saline, 2. MSN, 3. Len/OVA/MSN, 4. Len/OVA/yMSN). (B) Schematic illustration of innate immune responses of macrophages induced by yMSNs. (C) Speculative map of the signaling pathway activated by Len/OVA/yMSN. (D) Heatmap of genes upregulated by Len/OVA/yMSN in macrophages ($n = 3$). (E) Quantitation of the major immune response−related genes in macrophages by Len/OVA/yMSN ($n = 3$). (F) Expression and quantitation of major proteins related to immune response pathways by Western blot ($n = 3$). All of the data are presented as the mean $\pm$ SD. *$P < 0.05$; **$P < 0.01$; ***$P < 0.001$.

expressing co-stimulatory signals (CD80/86) were necessary for inducing a strong tumor-specific CTL response. This result was further supported by an *in vivo* CD8$^+$ T cell assay, where OVA-specific CD8$^+$ T cells in mesenteric lymph nodes showed 3.1-fold higher proliferation (Fig. 7D) when induced by Len/OVA/yMSNs than Len/OVA/MSNs. Moreover, systemic immune efficacy was explored. As shown in Fig. 7E, mice vaccinated with Len/OVA/yMSNs (*p.o.*) generated significantly higher titers of OVA-specific IgG when compared with mice vaccinated with OVA (*p.o.*) and Len/OVA/MSNs (*p.o.*) on Day 21 after immunization. Moreover, the titers of OVA-specific IgG from the sera of vaccinated mice exhibited a sharp increase on Day 28.

This was a positive feedback effect on adaptive immunity after promoting innate immunity, which would be beneficial to kill tumors, form immune memory, and prevent tumor recurrence. Altogether, we conclude that oral Len/OVA/yMSNs were able to induce robust specific CTLs and specific antibodies with

comparable or better efficacy than traditional OVA delivered *via* a subcutaneous route. In short, Len/OVA/yMSNs were not only a good delivery system for subunit antigens but they also acted as adjuvants to increase immunogenicity.

3.5. Antitumor efficacy and long-term immune-memory effects

Based on the above-described properties of Len/OVA/yMSNs, we then investigated their antitumor efficacy and long-term memory effect in an OVA-Hepa1-6 tumor-bearing C57BL/6 mice model (Fig. 8A). During a 14-day treatment based on the clinical trial protocol of lenvatinib (Synonyms: E7080), a significantly stronger inhibition effect was observed in the Len/OVA/yMSN group (89.5%) compared with other groups (Fig. 8B), among which the order of therapeutic efficacy from strong to weak was Len/yMSNs + OVA/yMSNs (49.8%), Len/yMSNs (45.8%), Len/OVA/MSNs (32.2%), Len (32.2%), and OVA/yMSNs (19.8%). OVA/
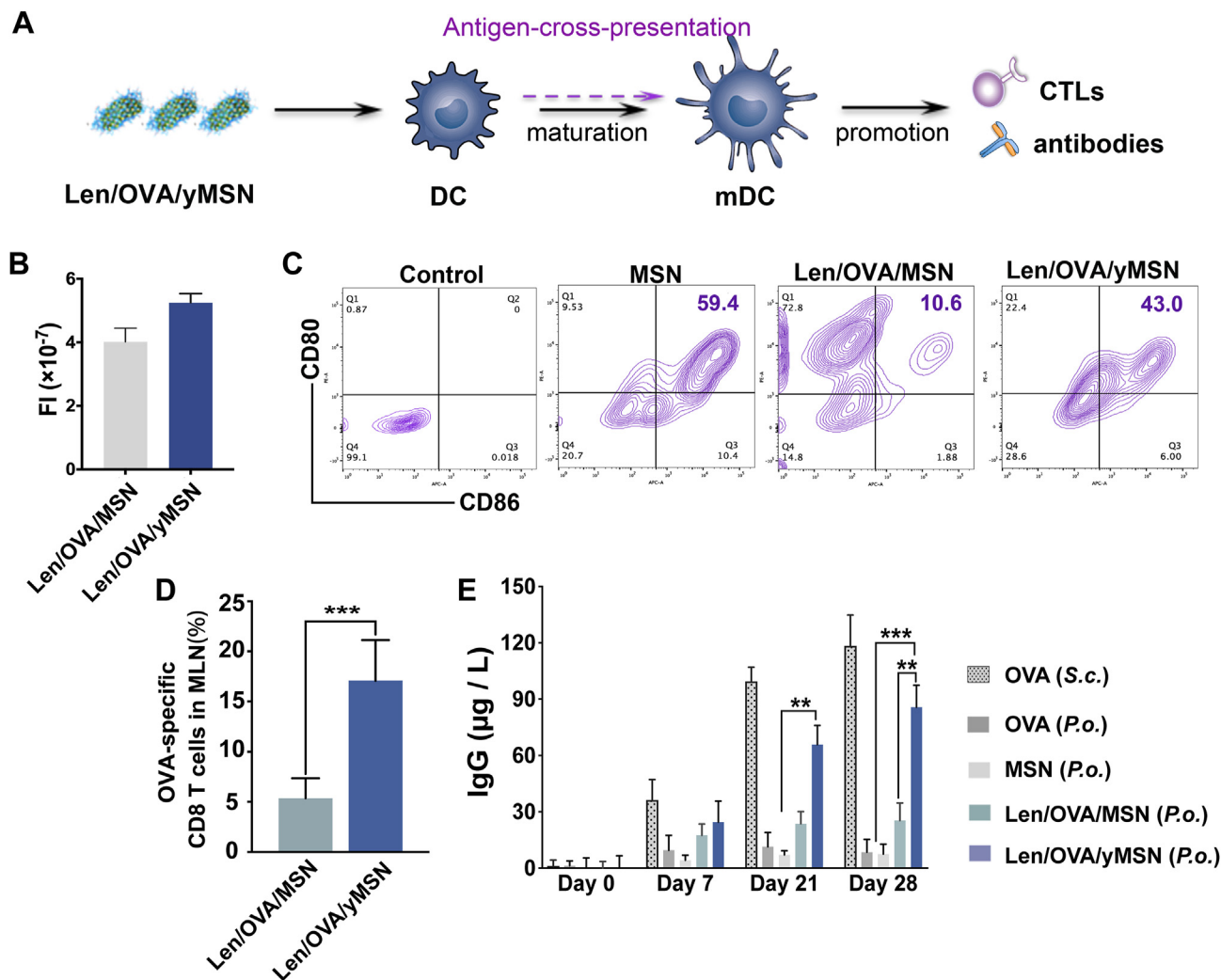
Figure 7 Adaptive immunomodulatory efficacy of the Len/OVA/yMSN on DCs. (A) Schematic illustration of adaptive immune responses of DCs induced by Len/OVA/yMSN. (B) FCM analysis of specific uptake of Len/OVA/yMSN uptake by BMDCs ($n = 3$). (C) FCM analysis of DC maturation promoted by Len/OVA/yMSNs. (D) Quantification of OVA-specific CD8$^+$ T cells in lymph nodes after oral Len/OVA/yMSN treatment by FCM ($n = 3$). (E) OVA-specific IgG antibody after 7, 21 and 28 days after vaccinations of the C57BL/6 mice with orally administrated (p.o.) of OVA solution, Len/OVA/MSN, Len/OVA/yMSN, and subcutaneous injection (s.c.) of OVA solution, respectively ($n = 3$). All of the data are presented as the mean ± SD. **$P < 0.01$; ***$P < 0.001$.

yMSNs did not result in a significant tumor reduction prior to Day 14, potentially leading to a great efficacy later because of the time needed for oral vaccination. Surprisingly, primary tumors regrew in these groups without OVA vaccination on Day 21, implying that the antiangiogenesis only depending on Len or innate immunotherapy by yMSNs could not eradicate tumors effectively. On the contrary, a continuous decrease was observed in both the Len/yMSN + OVA/yMSN group and the Len/OVA/yMSN group, while this delayed the decrease in the OVA/yMSN group, which had a tumor-inhibition rate of 81.9%, probably due to oral vaccination, which might take a certain time to initiate a robust specific immune response. Strictly speaking, Len/OVA/yMSNs achieved the maximum therapeutic efficacy (98.8%) rather than the mixture of Len/yMSNs and OVA/yMSNs (93.7%) (Fig. 8D and Supporting Information Fig. S7), further indicating the synergistic effect of targeting delivery of TKIs and therapeutic cancer vaccines. In complement to this, a terminal deoxynucleotidyl transferase dUTP nick-end labeling (TUNEL) analysis of these

excised tumors following treatment further revealed that Len/OVA/yMSNs obviously induced apoptosis and necrosis of these primary tumors (Fig. 8E).

Next, these tumor-excised mice were then rechallenged with 1×10^6 Hepa1-6 cells or OVA-Hepa1-6 cells at the left posterior hip of these mice to further investigate the specific immune effect on antitumor therapy. As shown in Fig. 8C, mice with previous treatments were resistant to these newly incubated tumor cells to different degrees. OVA/yMSNs, Len/OVA/yMSNs, and Len/yMSN + OVA/yMSNs all exerted significantly higher resistance to OVA-Hepa1-6 cells compared with other formulations without an OVA vaccine, suggesting a long-term antitumor effect in mice treated with OVA vaccines. Interestingly, tumor-excised mice rechallenged with hepa1-6 cells did not show any resistance to the newly incubated tumor cells in all groups, further indicating that only stimulating innate immune responses depending on yMSNs was not sufficient to fight cancer. Immune memory effect is crucial for preventing tumor recurrence and distant metastasis, and the
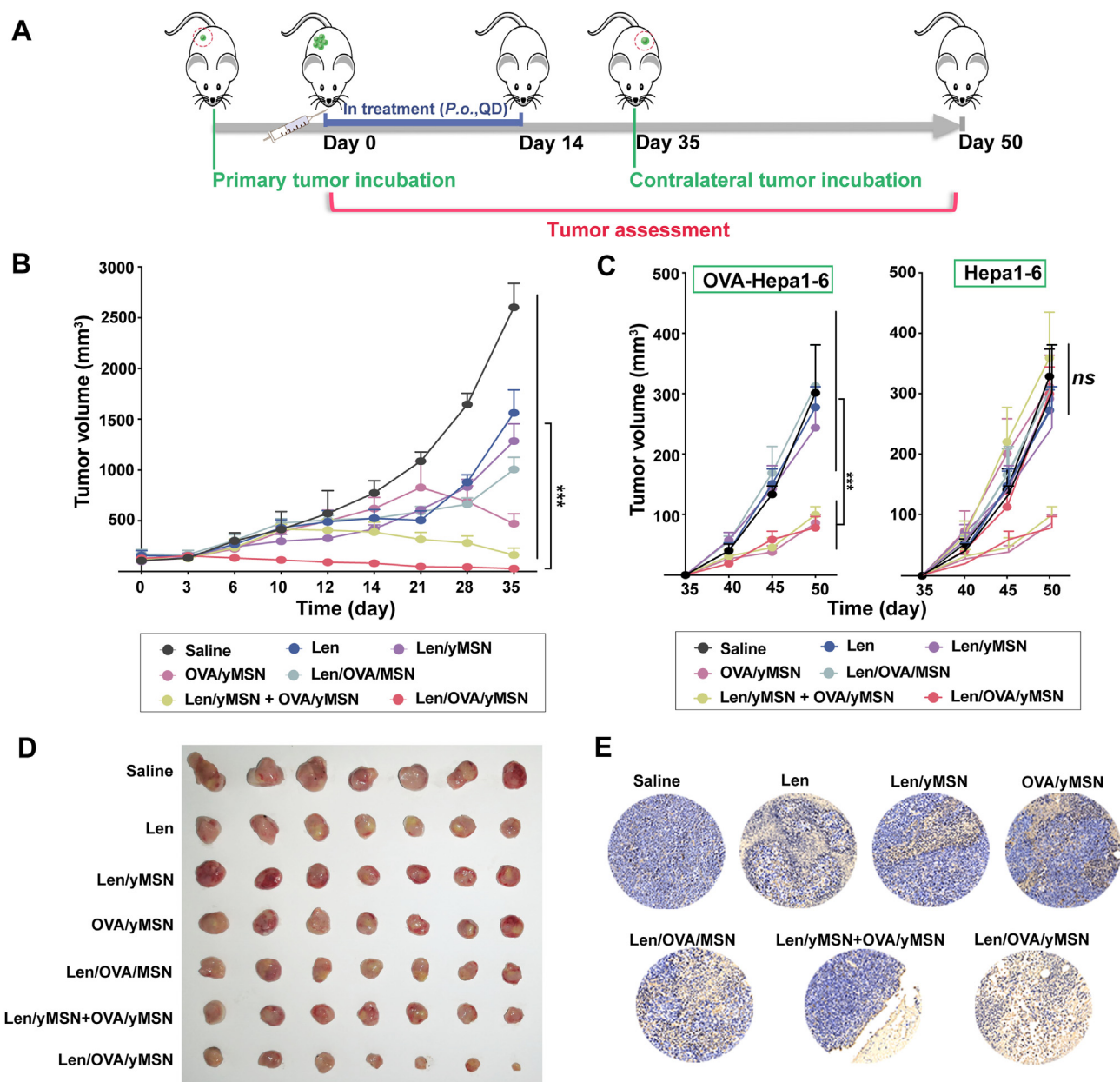
Figure 8 Antitumor efficacy and long-term antigen-specific immune-memory effects of Len/OVA/yMSNs. (A) Experimental schedule for Len/OVA/yMSN therapy. (B) Tumor growth curves of primary OVA-Hepa1-6 tumors in C57BL/6 mice ($n = 7$). (C) Rechallenged OVA-Hepa1-6 tumors and Hepa1-6 tumors removed from C57BL/6 mice after different treatments ($n = 7$). (D) Subcutaneous tumors after treatment courses. (E) Analysis of tumors apoptosis after treatment as shown by TUNEL detection. All of the data are presented as the mean $\pm$ SD. $*P < 0.05$; $**P < 0.01$; $***P < 0.001$. *ns*, not significance.

adaptive immune responses induced by our Len/OVA/yMSNs showed a promising long-term memory effect on tumor rechallenge.

3.6. Antitumor mechanism of Len/OVA/yMSNs in combination immunotherapy

Len is an oral multi-targeted tyrosine kinase inhibitor of VEGFR1-3, FGFR1-4, PDGFR-β, Ret, and KIT. Previous reports revealed that a potential advantage of Len is that it can inhibit multiple angiogenesis stimulatory pathways by blocking different signal transduction[48,49]. Thus, checking the expression of CD31 involved in angiogenesis may reflect the antitumor efficacy of Len more intuitively. To clarify the crucial role of Len in the highly efficient therapeutic performance of Len/OVA/yMSNs, we measured the CD31 expression in tumors. Immunohistochemistry analysis (Fig. 9A) showed that tumors treated with Len/OVA/yMSNs exhibited the lowest levels of CD31 (1.31%), indicating that these nanoparticles had greatest inhibitory effect on angiogenesis in tumors. Moreover, a large necrotic area was observed in the center of each tumor, probably due to angiogenic inhibition resulting in insufficient supplies of blood and nutrition. In addition, Len/yMSNs also lowered CD31 expression (1.90%) in tumors more significantly than Len alone (3.78%) or Len/OVA/MSNs (2.73%), implying that the tumor-targeting delivery of Len by yMSNs contributed to highly efficient therapeutic performance.
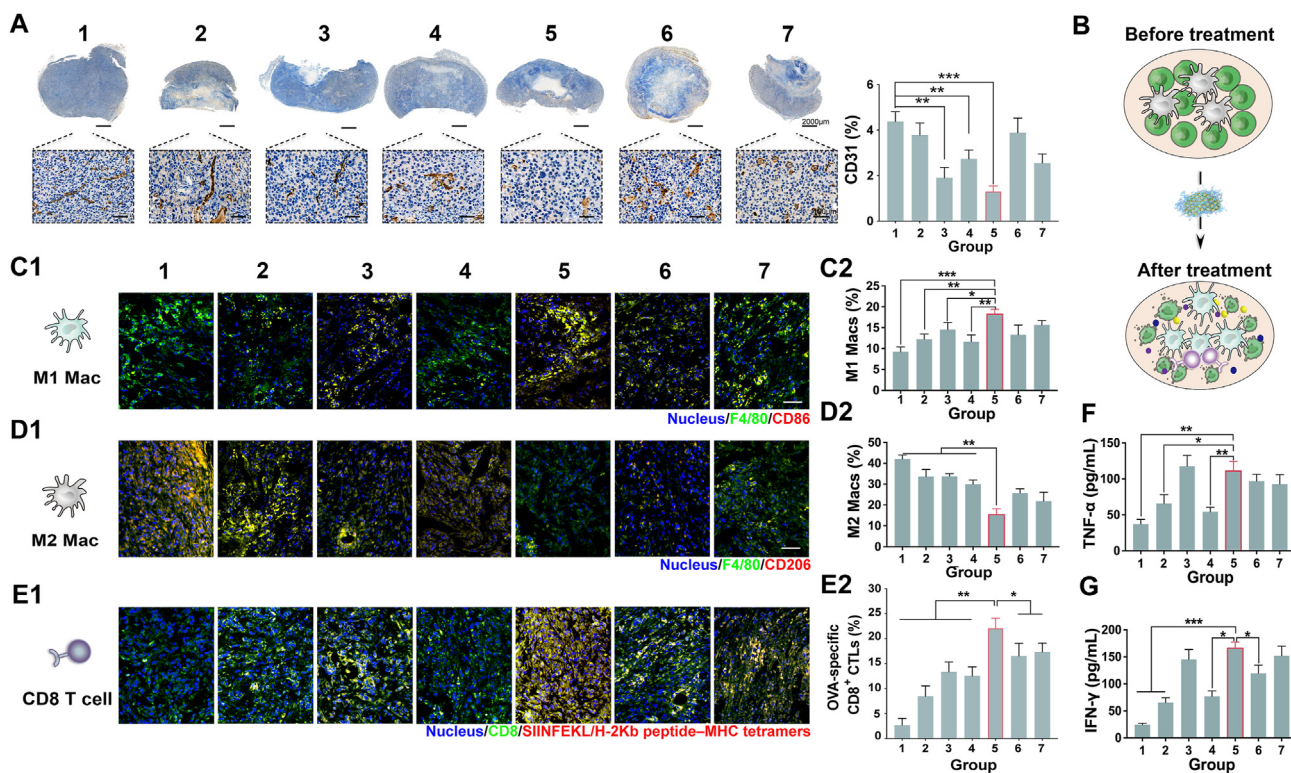
Figure 9 Antitumor mechanism of Len/OVA/yMSNs. (A) Immunohistochemical images and quantitative analysis of CD31 expression in tumors after 14 days of treatment ($n = 3$). (B) Schematic of TME after treatment, in which prime M2 macrophages could revert to M1 phenotype, OVA-specific CD8+ T cells could infiltrate tumors, and antitumoral cytokines could be secreted. (C−E) Immunofluorescence images of the tumors showing the polarization of M1 macrophages (C1), M2 macrophages (D1) and the infiltration of OVA-specific CD8$^+$ T cells (E1) in different treatment groups; scale bar = 100 μm. FCManalysis of the tumors showing the ratio of M1 macrophages (C2), M2 macrophages (D2) and infiltration of OVA-specific CD8$^+$ T cells (E2) in different treatment groups ($n = 3$). (F, G) ELISA analysis of Len/OVA/yMSN-induced secretion of proinflammatory cytokines including TNF-α and INF-γ in tumors ($n = 3$). Groups 1−7 respectively represent 1-saline, 2-Len, 3-Len/yMSNs, 4-Len/OVA/MSNs, 5-Len/OVA/yMSNs, 6-OVA/yMSNs, and 7-Len/yMSNs + OVA/yMSNs. All of the data are presented as the mean ± SD. ***$P < 0.001$. ns, not significance.

In addition to the antitumor efficacy of Len, the considerable contributions of the OVA vaccine and yMSN to antitumor immunotherapy could not be ignored. We therefore explored changes in the TMEs of Hepa1-6/OVA tumor-bearing mice treated with different formulations—reversion of prime M2 macrophages to the M1 phenotype, infiltration of OVA-specific CD8$^+$ T cells, and secretion of antitumor cytokines (Fig. 9B)—to reveal the specific contributions of OVA and yMSNs. Effective macrophagic activation is critical to robust immune response[50]. Theoretically, highly activated M1 macrophages can revert neighbor M2 phenotype towards M1 phenotype through cytokine-mediated intercellular communication[51]. In our system, there might have been another strong driver of M2-to-M1 reversion in macrophages, that is the *Saccharomyces*-glucan coating on the surface of our MSNs. Therefore, we explored whether yMSN could withstand immunosuppression in the TME. We first performed CD86 (a marker of M1-macrophages) immunofluorescence staining and flow cytometric examination to investigate the influences on the M1-macrophages inside tumor tissues (Fig. 9C). Apparently, the largest increase in M1 macrophages was observed inside the tumors treated with Len/OVA/yMSNs (18.2%). We also performed CD206 (a marker of M2-macrophages) immunofluorescence staining to investigate the influences on the M2-macrophages inside tumor tissues (Fig. 9D). All groups with yMSNs, including Len/yMSNs, OVA/yMSNs, Len/yMSNs + OVA/yMSNs, and Len/OVA/yMSNs, resulted in an apparent reduction in the number of CD206$^+$ cells (Len/yMSN: 33.7%, OVA/yMSN: 25.7%, Len/yMSN + OVA/yMSN: 21.8%, Len/OVA/yMSN: 15.4%) when compared with saline (42.00%), providing convincing *in vivo* evidence to support the conclusion that yMSNs could effectively reverse M2 macrophages within tumors to M1 phenotype. Encouragingly, the simultaneous elimination of M2-TAMs ensured that activated cytotoxic T cells (CTLs) exert antitumor immunity within tumors *via* decreasing immunosuppressive cytokine secretion and tumor infiltration of Treg cells[52]. Then, the intratumoral infiltration of OVA-specific CD8 CTLs (SIINFEKL/H-2Kb peptide−MHC tetramers$^+$ cells) was then examined by immunofluorescence and flow cytometric examination of tumors. As shown in Fig. 9E, OVA/yMSNs and Len/yMSNs + OVA/yMSNs induced comparable OVA-specific CD8 CTL infiltration ratios (27.8% and 30.6%, respectively), which were 3.5-fold and 3.8-fold higher than saline (8.0%), respectively. Interestingly, Len/yMSNs exhibited a significantly higher OVA-specific CD8 CTL infiltration ratio (24.0%) than Len alone (14.8%), but this was lower than OVA/yMSNs (27.8%), indicating that yMSNs play a promotive role in DC maturation and antigen-cross-presenting, which was in accordance with previous results *in vitro*. Moreover, Len/OVA/yMSNs further increased the frequency of OVA-specific CD8 CTLs to 39.1%, which was 4.9-fold

higher than saline, efficiently promoting the infiltration of CLTs into solid tumors by decreasing immunosuppression[53]. Of note, the significant increase between Len/OVA/yMSNs and a mixture of Len and OVA/yMSNs further validated the synergistic effect of this combination of Len and OVA in yMSNs. Moreover, the secreted inflammatory factors could also work as signal factors, responsible for cancer cell killing and leukocyte recruitment[54]. Therefore, the induction of immune responses in the tumor microenvironment was then evaluated by measuring the intratumor concentrations of proinflammatory cytokines using ELISA. The combination of Len or OVA with yMSNs (Len/yMSNs, OVA/yMSNs, Len/yMSNs + OVA/yMSNs, and Len/OVA/yMSNs) all significantly promoted the secretion of IFN-γ and TNF-α in tumors. For instance, the concentrations of IFN-γ and TNF-α induced by Len/OVA/yMSNs were 3.0-, 1.7-, and 2.1-fold higher than those of saline, Len alone, and Len/OVA/MSNs, respectively, indicating the successful elicitation of robust antitumor immune responses triggered by yMSNs itself (Fig. 9F and G).

A gastrointestinal irritation evaluation was then carried out to ensure that the safety of Len/OVA/yMSN. As a result, no histopathological lesions or hyperemia were observed in all treatment groups (Supporting Information Fig. S8). Furthermore, the changes in body weight of OVA-Hepa1-6 tumor-bearing C57BL/6 mice during treatment, hematoxylin-eosin (H&E) staining of major organs (*i.e.*, heart, lung, liver, spleen, and kidney), and hematological and biochemical analysis of the serum at the end of antitumor studies together revealed that Len/OVA/yMSNs had good biosafety and did not cause any histological damage to the major organs (Supporting Information Figs. S9 and S10, and Tables S4 and S5).

4. Conclusions

In summary, we have engineered a novel *Saccharomyces*-inspired nanoparticle with multiple functions that i) precisely delivers small molecules to tumors through oral route for a high efficacy and low toxicity; ii) effectively delivers protein antigens to resident antigen-presenting cells within lymphoid tissues after oral administration for stronger immunization; and iii) safely awakens innate immune responses by activating the TLR2/4-signaling pathway, strengthening vaccine-induced immune responses and reversing macrophage-associated immunosuppression in the TME. Finally, Len/OVA/yMSNs exerted a tremendous and long-term synergistic effect in the treatment of hepatic carcinoma by causing significant antiangiogenic effects and efficient resistance against intratumoral immunosuppression, without adverse side effects. These characteristics of yMSNs allow them to package other tumor neo-antigens as therapeutic cancer vaccines and chemotherapeutic agents for potential combination antitumor therapy. Moreover, such a high-performance nanocarrier provides an innovative approach for lesion-targeting delivery of oral drugs accompanied with the awakening of the innate/adaptive immunity of the body and the lesion environment.

Acknowledgments

Author contributions

Yuling Mao designed and performed the experiments, analyzed and interpreted the data, and wrote the manuscript. Xiudan Wang, Caishun Chen and Qinfu Zhao assisted to finish the experiment. Yanfeng Liu and Jinghai Zhang guided parts of molecular biology experiments. Siling Wang conceived and supervised the project and analyzed and interpreted the data.

Conflicts of interest

The authors have no conflicts of interest to declare.

Appendix A. Supporting information

Supporting data to this article can be found online at https://doi.org/10.1016/j.apsb.2022.04.018.

References

1. Zhou SB, Gravekamp C, Bermudes D, Liu K. Tumour-targeting bacteria engineered to fight cancer. *Nat Rev Cancer* 2018;**18**:727−43.
2. Ruan CH, Liu LS, Lu YF, Zhang Y, He X, Chen XL, et al. Substance P-modified human serum albumin nanoparticles loaded with paclitaxel for targeted therapy of glioma. *Acta Pharm Sin B* 2018;**8**:85−96.
3. Riley RS, June CH, Langer R, Mitchell MJ. Delivery technologies for cancer immunotherapy. *Nat Rev Drug Discov* 2019;**18**:175−96.
4. Pierige F, Serafini S, Rossi L, Magnani M. Cell-based drug delivery. *Adv Drug Deliv Rev* 2008;**60**:286−95.
5. Nam J, Son S, Park KS, Zou WP, Shea LD, Moon JJ. Cancer nanomedicine for combination cancer immunotherapy. *Nat Rev Mater* 2019;**4**:398−414.
6. Soares KC, Rucki AA, Wu AA, Olino K, Xiao Q, Chai Y, et al. PD-1/PD-L1 blockade together with vaccine therapy facilitates effector T-cell infiltration into pancreatic tumors. *J Immunother* 2015;**38**:1−11.
7. Matsushita H, Vesely MD, Koboldt DC, Rickert CG, Uppaluri R, Magrini VJ, et al. Cancer exome analysis reveals a T-cell-dependent mechanism of cancer immunoediting. *Nature* 2012;**482**:400−4.
8. Mao YL, Feng S, Li S, Zhao QF, Di DH, Liu YF, et al. Chylomicron-pretended nano-bio self-assembling vehicle to promote lymphatic transport and GALTs target of oral drugs. *Biomaterials* 2019;**188**:173−86.
9. Yanez JA, Wang SW, Knemeyer IW, Wirth MA, Alton KB. Intestinal lymphatic transport for drug delivery. *Adv Drug Deliv Rev* 2011;**63**:923−42.
10. Zhang ZC, Lu Y, Qi JP, Wu W. An update on oral drug delivery *via* intestinal lymphatic transport. *Acta Pharm Sin B* 2021;**11**:2449−68.
11. Xue JW, Zhao ZK, Zhang L, Xue LJ, Shen SY, Wen YJ, et al. Neutrophil-mediated anticancer drug delivery for suppression of postoperative malignant glioma recurrence. *Nat Nanotechnol* 2017;**12**:692−700.
12. Jiang W, von Roemeling CA, Chen YX, Qie YQ, Liu XJ, Chen JZ, et al. Designing nanomedicine for immuno-oncology. *Nat Biomed Eng* 2017;**1**:29.
13. Wershil BK, Furuta GT. 4. Gastrointestinal mucosal immunity. *J Allergy Clin Immunol* 2008;**121**:S380−3. quiz S415.
14. Cai ZY, Sanchez A, Shi ZC, Zhang TT, Liu MY, Zhang DK. Activation of toll-like receptor 5 on breast cancer cells by flagellin suppresses cell proliferation and tumor growth. *Cancer Res* 2011;**71**:2466−75.
15. Zhang XJ, Xu XQ, Chen YD, Dou Y, Zhou X, Li LL, et al. Bioinspired yeast microcapsules loaded with self-assembled nanotherapies for

targeted treatment of cardiovascular disease. *Mater Today* 2017;**20**:301−13.

16. Zhou X, Zhang XJ, Han SL, Dou Y, Liu MY, Zhang L, et al. Yeast microcapsule-mediated targeted delivery of diverse nanoparticles for imaging and therapy *via* the oral route. *Nano Lett* 2017;**17**:1056−64.

17. Vela Ramirez JE, Sharpe LA, Peppas NA. Current state and challenges in developing oral vaccines. *Adv Drug Deliv Rev* 2017;**114**:116−31.

18. Fan JX, Li ZH, Liu XH, Zheng DW, Chen Y, Zhang XZ. Bacteria-mediated tumor therapy utilizing photothermally-controlled TNF-α expression *via* oral administration. *Nano Lett* 2018;**18**:2373−80.

19. Hu QL, Wu M, Fang C, Cheng CY, Zhao MM, Fang WH, et al. Engineering nanoparticle-coated bacteria as oral DNA vaccines for cancer immunotherapy. *Nano Lett* 2015;**15**:2732−9.

20. Brown TD, Whitehead KA, Mitragotri S. Materials for oral delivery of proteins and peptides. *Nat Rev Mater* 2020;**5**:127−48.

21. Akira S, Takeda K, Kaisho T. Toll-like receptors: critical proteins linking innate and acquired immunity. *Nat Immunol* 2001;**2**:675−80.

22. Demir G, Klein HO, Mandel-Molinas N, Tuzuner N. Beta glucan induces proliferation and activation of monocytes in peripheral blood of patients with advanced breast cancer. *Int Immunopharm* 2007;**7**:113−6.

23. Li W, Liu ZH, Fontana F, Ding YP, Liu DF, Hirvonen JT, et al. Tailoring porous silicon for biomedical applications: from drug delivery to cancer immunotherapy. *Adv Mater* 2018;**30**:e1703740.

24. Wang KL, Lu JY, Li JL, Gao YL, Mao YL, Zhao QF, et al. Current trends in smart mesoporous silica-based nanovehicles for photo-activated cancer therapy. *J Control Release* 2021;**339**:445−72.

25. Shumaker R, Aluri J, Fan J, Martinez G, Pentikis H, Ren M. Influence of hepatic impairment on lenvatinib pharmacokinetics following single-dose oral administration. *J Clin Pharmacol* 2015;**55**:317−27.

26. Naglieri E. Management of toxicity in patients treated with tyrosine kinase inhibitors (TKI). *Eur J Cancer Suppl* 2008;**6**:42−5.

27. Zhang TL, Lu ZG, Wang JZ, Shen J, Han QL, Li Y, et al. Preparation of hollow mesoporous silica nanoparticles with tunable pore diameters for encapsulating and slowly releasing eugenol. *Chin Chem Lett* 2020;**31**:3135−8.

28. Mao YL, Han MQ, Chen CS, Wang XD, Han JN, Gao YK, et al. A biomimetic nanocomposite made of a ginger-derived exosome and an inorganic framework for high-performance delivery of oral antibodies. *Nanoscale* 2021;**13**:20157−69.

29. Sha LP, Zhao QF, Wang D, Li X, Wang XD, Guan XY, et al. "Gate" engineered mesoporous silica nanoparticles for a double inhibition of drug efflux and particle exocytosis to enhance antitumor activity. *J Colloid Interface Sci* 2019;**535**:380−91.

30. Zhang WZ, Wang MZ, Tang W, Wen R, Zhou SY, Lee CB, et al. Nanoparticle-laden macrophages for tumor-tropic drug delivery. *Adv Mater* 2018;**30**:e1805557.

31. Luo M, Wang H, Wang ZH, Cai HC, Lu ZG, Li Y, et al. A STING-activating nanovaccine for cancer immunotherapy. *Nat Nanotechnol* 2017;**12**:648−54.

32. De Smet R, Demoor T, Verschuere S, Dullaers M, Ostroff GR, Leclercq G, et al. β-Glucan microparticles are good candidates for mucosal antigen delivery in oral vaccination. *J Control Release* 2013;**172**:671−8.

33. Brown GD, Taylor PR, Reid DM, Willment JA, Williams DL, Martinez-Pomares L, et al. Dectin-1 is a major beta-glucan receptor on macrophages. *J Exp Med* 2002;**196**:407−12.

34. Brown GD, Gordon S. Immune recognition. A new receptor for beta-glucans. *Nature* 2001;**413**:36−7.

35. Hong F, Yan J, Baran JT, Allendorf DJ, Hansen RD, Ostroff GR, et al. Mechanism by which orally administered beta-1,3-glucans enhance the tumoricidal activity of antitumor monoclonal antibodies in murine tumor models. *J Immunol* 2004;**173**:797−806.

36. Mosser DM, Edwards JP. Exploring the full spectrum of macrophage activation. *Nat Rev Immunol* 2008;**18**:958−69.

37. Zhao YH, Chu X, Chen JT, Wang Y, Gao SJ, Jiang YX, et al. Dectin-1-activated dendritic cells trigger potent antitumour immunity through the induction of Th9 cells. *Nat Commun* 2016;**7**:12368.

38. Zhou X, Ling KJ, Liu MY, Zhang XJ, Ding J, Dong Y, et al. Targeted delivery of cisplatin-derived nanoprecursors *via* a biomimetic yeast microcapsule for tumor therapy by the oral route. *Theranostics* 2019;**9**:6568−86.

39. Miyagi T, Takehara T, Tatsumi T, Suzuki T, Jinushi M, Kanazawa Y, et al. Concanavalin a injection activates intrahepatic innate immune cells to provoke an antitumor effect in murine liver. *Hepatology* 2004;**40**:1190−6.

40. Chanmee T, Ontong P, Konno K, Itano N. Tumor-associated macrophages as major players in the tumor microenvironment. *Cancers* 2014;**6**:1670−90.

41. Lewis CE, Harney AS, Pollard JW. The multifaceted role of perivascular macrophages in tumors. *Cancer Cell* 2016;**30**:18−25.

42. Pyonteck SM, Akkari L, Schuhmacher AJ, Bowman RL, Sevenich L, Quail DF, et al. CSF-1R inhibition alters macrophage polarization and blocks glioma progression. *Nat Med* 2013;**19**:1264−72.

43. Hodge JW, Ardiani A, Farsaci B, Kwilas AR, Gameiro SR. The tipping point for combination therapy: cancer vaccines with radiation, chemotherapy, or targeted small molecule inhibitors. *Semin Oncol* 2012;**39**:323−39.

44. Murray PJ, Wynn TA. Protective and pathogenic functions of macrophage subsets. *Nat Rev Immunol* 2011;**11**:723−37.

45. Hong XY, Zhong XF, Du GS, Hou YY, Zhang YT, Zhang ZR, et al. The pore size of mesoporous silica nanoparticles regulates their antigen delivery efficiency. *Sci Adv* 2020;**6**:eaaz4462.

46. Wang XP, Li X, Ito A, Watanabe Y, Sogo Y, Tsuji NM, et al. Stimulation of *in vivo* antitumor immunity with hollow mesoporous silica nanospheres. *Angew Chem Int Ed Engl* 2016;**55**:1899−903.

47. Cha BG, Jeong JH, Kim J. Extra-large pore mesoporous silica nanoparticles enabling co-delivery of high amounts of protein antigen and Toll-like receptor 9 agonist for enhanced cancer vaccine efficacy. *ACS Cent Sci* 2018;**4**:484−92.

48. Bruheim S, Kristian A, Uenaka T, Suo Z, Tsuruoka A, Nesland JM, et al. Antitumour activity of oral E7080, a novel inhibitor of multiple tyrosine kinases, in human sarcoma xenografts. *Int J Cancer* 2011;**129**:742−50.

49. Matsuki M, Adachi Y, Ozawa Y, Kimura T, Hoshi T, Okamoto K, et al. Targeting of tumor growth and angiogenesis underlies the enhanced antitumor activity of lenvatinib in combination with everolimus. *Cancer Sci* 2017;**108**:763−71.

50. Guerriero JL, Sotayo A, Ponichtera HE, Castrillon JA, Pourzia AL, Schad S, et al. Class IIa HDAC inhibition reduces breast tumours and metastases through anti-tumour macrophages. *Nature* 2017;**543**:428−32.

51. Mantovani A, Sica A, Sozzani S, Allavena P, Vecchi A, Locati M. The chemokine system in diverse forms of macrophage activation and polarization. *Trends Immunol* 2004;**25**:677−86.

52. Deng CF, Zhang Q, Jia MD, Zhao J, Sun X, Gong T, et al. Tumors and their microenvironment dual-targeting chemotherapy with local immune adjuvant therapy for effective antitumor immunity against breast cancer. *Adv Sci* 2019;**6**:1801868.

53. Farsaci B, Donahue RN, Coplin MA, Grenga I, Lepone LM, Molinolo AA, et al. Immune consequences of decreasing tumor vasculature with antiangiogenic tyrosine kinase inhibitors in combination with therapeutic vaccines. *Cancer Immunol Res* 2014;**2**:1090−102.

54. Yu M, Duan XH, Cai YJ, Zhang F, Jiang SQ, Han SS, et al. Multifunctional nanoregulator reshapes immune microenvironment and enhances immune memory for tumor immunotherapy. *Adv Sci* 2019;**6**:1900037.